

Parvalbumin-Expressing Interneurons in the BTBR T^+ *Itpr3^{tf}*/J Idiopathic Mouse Model of Autism Spectrum Disorder

By

Krystian Wiktor Pięta | BSc

A thesis submitted in partial fulfilment of the requirements for the degree of
MSc (by Research) at the University of Central Lancashire (UCLan)

September 2023

RESEARCH STUDENT DECLARATION FORM

Type of Award MSc (by Research)
School Psychology and Humanities

1. Concurrent registration for two or more academic awards

I declare that while registered as a candidate for the research degree, I have not been a registered candidate or enrolled student for another award of the University or other academic or professional institution.

2. Material submitted for another award

I declare that no material contained in the thesis has been used in any other submission for an academic award and is solely my own work.


3. Collaboration

Where a candidate's research programme is part of a collaborative project, the thesis must indicate in addition clearly the candidate's individual contribution and the extent of the collaboration. Please state below:

N/A

4. Use of a Proof-reader

No proofreading service was used in the compilation of this thesis.

Signature of Candidate: 

Print name: KRYSTIAN PIETA



ABSTRACT

Parvalbumin (PV)-expressing inhibitory interneurons are considered critical in regulating excitation/inhibition (E/I) balance and have gained particular interest in the aetiology of autism spectrum disorder (ASD). Dysfunction of the dorsal striatum has been profoundly associated with ASD aetiology, regions which are involved in goal-directed and habitual behaviour in the dorsomedial (DMS) and dorsolateral striatum (DLS), respectively. Perineuronal nets (PNNs) are extracellular structures which predominantly surround PV⁺ interneurons and contribute to their fast-spiking properties. Utilising the BTBR $T^+ Itpr3^{fl}/J$ (BTBR) mouse model of ASD, we investigated whether this idiopathic strain exhibits a reduced expression of PV. Through immunohistochemistry, we observed that BTBR mice had a reduced density of PV⁺ interneurons in the DMS, whilst density of PNNs was unaltered. The percentage of VVA⁺ cells with PV expression as well as PV levels were found to be significantly decreased, suggesting that BTBR mice present with a downregulation of PV expression in the DMS. We observed that control mice have a greater percentage of PV⁺ interneurons with PNNs in the DLS than in the DMS, however, BTBR mice were found to not possess such a gradient. We also observed that colocalisation of PV⁺ interneurons with PNNs in the dorsal striatum was higher in female BTBR mice than in male counterparts. This sex difference was not evident in control mice. PV downregulation may be a common endpoint of ASD aetiology in an idiopathic, and other, mouse models of ASD. Alterations in the colocalisation of PV⁺ interneurons with PNNs alongside PV reduction have been shown to alter neuronal function and we anticipate that such may also alter E/I balance in BTBR mice. Differences which prevail between sexes in BTBR mice highlight the importance of considering sex in the aetiology of ASD and BTBR may be a particular robust strain to further investigate this.

Keywords: Parvalbumin, BTBR, Excitation/Inhibition, Autism Spectrum Disorder, Perineuronal net, Dorsomedial Striatum, Dorsolateral Striatum

CONTENTS

ABSTRACT.....	iii
CONTENTS	iv
LIST OF TABLES.....	vi
LIST OF FIGURES	vi
LIST OF APPENDICES	viii
ACKNOWLEDGEMENTS	ix
ABBREVIATIONS	x
1.0 INTRODUCTION.....	1
1.1 Striatal Dysfunction in ASD.....	1
1.2 Dorsomedial and Dorsolateral Striatum Subregions	2
1.3 Excitation and Inhibition Balance	3
1.4 Parvalbumin-Expressing Interneurons	4
1.5 Loss of Pvalb Interneurons or Reduced PV Expression?	5
1.6 Idiopathic Mouse Model of ASD.....	6
1.7 Sex Differences in ASD and BTBR mice.....	7
1.8 Experimental Aims.....	8
1.9 Hypotheses	10
2.0 MATERIALS AND METHODS.....	11
2.1 Animals	11
2.2 Tissue Dissection	11
2.3 Tissue Preparation and Immunohistochemistry	13
2.3 Tissue Selection	13
2.4 Image Acquisition & Region of Interest Selection.....	15
2.5 Counting Criteria.....	17
2.6 Cell Density & Colocalisation Percentage	18
2.7 Protein Lysate Preparation	18
2.8 BCA Protein Assay	18
2.9 SDS-PAGE Gel Electrophoresis	19
2.10 Wet Transfer.....	20
2.11 Western blotting.....	20
2.12 Blot Quantification	21

2.13 Statistical Analysis	21
3.0 RESULTS	22
3.1 Immunohistochemistry - Dorsal Striatum	22
3.2 Subregional & Sex Differences	27
3.3 Subregional & Sex Differences in C57 mice	28
3.4 Subregional & Sex Differences in BTBR mice	31
3.5 Dorsomedial Striatum	35
3.6 Dorsolateral Striatum	39
3.7 Western Blotting - PV Expression in the Striatum of BTBR mice	42
3.8 Summary Table of Results	43
4.0 DISCUSSION.....	45
4.1 Decreased PV expression, but unaltered density of Pvalb interneurons in the dorsal striatum of BTBR mice.....	45
4.2 Dorsomedial striatum accounts for reduction in PV expression in BTBR mice	46
4.3 Control mice have a higher percentage of PV+ cells surrounded by PNNs in DLS than DMS	47
4.4 Sex differences in BTBR mice - altered colocalisation of PV+ interneurons with perineuronal nets.....	49
4.5 Limitations and Future Directions	50
5.0 CONCLUSION	51
6.0 REFERENCES	52
7.0 APPENDICES	64

LIST OF TABLES

Table 1 Mean and standard deviation (SD) of PV+ cell density (cells/mm ²) in the Dorsal Striatum of male and female, C57 and BTBR mice.	22
Table 2 Mean and standard deviation (SD) of VVA+ cell density (cells/mm ²) in the Dorsal Striatum of male and female, C57 and BTBR mice.	22
Table 3 Mean and standard deviation (SD) of Percentage of VVA+ cells with PV expression in the Dorsal Striatum of male and female, C57 and BTBR mice.	22
Table 4 Mean and standard deviation (SD) of Percentage of PV+ cells surrounded by VVA in the Dorsal Striatum of male and female, C57 and BTBR mice.	23
Table 5 Mean and standard deviation (SD) of PV+ cell density (cells/mm ²) in the Dorsomedial (DMS) and Dorsolateral Striatum (DMS) of male and female, C57 and BTBR mice.....	27
Table 6 Mean and standard deviation (SD) of VVA+ cell density (cells/mm ²) in the Dorsomedial (DMS) and Dorsolateral Striatum (DMS) of male and female, C57 and BTBR mice.....	27
Table 7 Mean and standard deviation (SD) Percentage of VVA+ cells with PV expression in the Dorsomedial (DMS) and Dorsolateral Striatum (DMS) of male and female, C57 and BTBR mice.....	28
Table 8 Mean and standard deviation (SD) Percentage of PV+ cells surrounded by VVA in the Dorsomedial (DMS) and Dorsolateral Striatum (DMS) of male and female, C57 and BTBR mice.....	28
Table 9 Summary table of results, linking to the hypotheses in this study and the relevant figure.....	43

LIST OF FIGURES

Figure 1 Mouse Brain Atlas adapted from Franklin and Paxinos (2007) with visual representation of striatal dissection procedure. (A) Sagittal section of mouse brain at 0.12mm lateral. Incisions made posterior of the genu of the corpus callosum (approx. 1.10mm bregma) and posterior of the anterior commissure and fornix (approx. -0.10mm bregma), yielded a disk which contained the striatum (shaded light blue). (B) Coronal section of mouse brain at 1.10mm bregma. Striatum (shaded light blue region) was dissected away from the cortex along the corpus callosum and septum along the lateral ventricle. Triangles indicate the corpus callosum (blue), genu of the corpus callosum (green), fornix (purple), anterior commissure (red), septal regions (yellow), and lateral ventricle (orange).	12
Figure 2 Mouse brain atlas adapted from Franklin and Paxinos (2007), indicating regions used to distinguish presence of the striatum. (A) Coronal section of mouse brain at 1.10mm bregma. (B) Coronal section of a mouse brain at -0.10mm bregma. Triangles	

indicate the striatum (grey), corpus callosum (green), lateral ventricle (blue), dorsal third ventricle (yellow), and anterior commissure (red). 14

Figure 3 | Representative PV immunofluorescence images from the striatum of a C57 mouse, visualising the selection process of ROIs (DMS and DLS). (A) Vertical 1mm measurement from the most dorsal region of the striatum was taken (under the corpus callosum; CC), after which a horizontal measurement captured the width of the dorsal striatum (DS) from the beginning of the lateral ventricle (LV) to the edge of the CC. (B) The diameter of the ROIs were determined by 35% of the DS width. DMS ROIs were determined, with close proximity, lateral to the LV and inferior to the CC. DLS ROIs were determined laterally to that of the DMS, without overlap, and close proximity to the CC. Scale bar: 500µm. 16

Figure 4 | Representative images of PV+ cells, VVA+ cells, and PV+VVA+ co-localisation from mouse dorsal striatum (DS), matching the predefined criteria. (A) PV+ cells (green), VVA+ cells (red), merged images showing PV and VVA overlapping in the DS of a C57 mouse. Slices were counterstained with DAPI (blue). (B) Enlarged images of the boxes outlined in A. White triangles point at in focus PV+VVA+ double positive cells, with a clearly stained DAPI nucleus. Scale bar: (A) 50µm; (B) 20µm. 17

Figure 5 | BCA assay standard curve of Bovine Serum Albumin (BSA) concentration (µg/µL) versus absorbance (AU). Absorbance measurements taken at a wavelength of 562nm. 19

Figure 6 | Bar charts showing, irrespective of sex, mean (±SD) PV+ cell density (A), mean (±SD) VVA+ cell density (B), mean (±SD) percentage of VVA+ cells with PV expression (C) and mean (±SD) percentage of PV+ cells surrounded by VVA (D) in the Dorsal Striatum of C57 (grey) and BTBR (white) mice. (E-H) Bar charts show differences between male and female mice. Asterisks represent * $p \leq 0.05$, ** $p \leq 0.01$ and *** $p \leq 0.001$, respectively. 26

Figure 7 | Bar charts showing mean (±SD) PV+ cell density (A), mean (±SD) VVA+ cell density (B), mean (±SD) percentage of VVA+ cells with PV expression (C), and mean (±SD) percentage of PV+ cells surrounded by VVA (D) in the Dorsomedial (DMS) and Dorsolateral Striatum (DLS) of male and female C57 mice. Asterisks represent * $p \leq 0.05$, ** $p \leq 0.01$, and *** $p \leq 0.001$, respectively 31

Figure 8 | Bar charts showing mean (±SD) PV+ cell density (A), mean (±SD) VVA+ cell density (B), mean (±SD) percentage of VVA+ cells with PV expression (C), and mean (±SD) percentage of PV+ cells surrounded by VVA (D) in the Dorsomedial (DMS) and Dorsolateral Striatum (DLS) of male and female C57 mice. Asterisks represent * $p \leq 0.05$, and *** $p \leq 0.001$, respectively. 34

Figure 9 | Bar chart showing mean (±SD) PV+ cell density (A), mean (±SD) VVA+ cell density (B), and mean (±SD) percentage of VVA+ cells with PV expression (C), and mean (±SD) percentage of PV+ cells surrounded by VVA (C) in the Dorsomedial Striatum (DMS) of male and female C57 (grey) and BTBR (white) mice. Asterisks represent * $p \leq 0.05$, ** $p \leq 0.01$, and *** $p \leq 0.001$, respectively (D) Representative immunofluorescence images of PV+ cells (white triangles) and VVA+ cells (yellow triangles) from the DMS of a C57 and BTBR mice with an approx. similar ROI area (mm²), counterstained with DAPI. Scale bar: 100µm 39

Figure 10 | Bar chart showing mean (\pm SD) PV+ cell density (A), mean (\pm SD) VVA+ cell density (B), and mean (\pm SD) percentage colocalisation of PV+VVA+ cells (C) in the Dorsolateral Striatum (DLS) of male and female C57 (grey) and BTBR (white) mice. Asterisks represent *** $p \leq 0.001$. (D) Representative immunofluorescence images of PV+ cells (white triangles), VVA+ cells (yellow triangles), and PV+VVA+ cells (white triangle with yellow border) from the DLS of a male C57 and male BTBR mice, counterstained with DAPI. Scale bar: 100 μ m. 42

Figure 11 | (A) Representative Western Blot and (B) quantification of PV levels in the male C57 and BTBR mice. β -actin was used as a loading control for the normalisation of the PV signal. Results are expressed as a percentage of normalised PV levels measured in control (C57), defined as 100%. Asterisks represent * $p \leq 0.05$. Data was collated from three independent experiments (two membranes per experiment) and shown as mean \pm SEM. 42

LIST OF APPENDICES

Appendix A | Link and QR code to the recording of mouse brain dissection. 64

Appendix B | Zeiss Cell Observer Filter Models' Excitation and Detection Wavelengths 64

Appendix C | Average Absorbance of each lysate, concentration (μ g/ μ L) determined using the BCA standard curve, and volume of lysate required to obtain 10 μ g of proteins (μ L). 64

Appendix D | Representative Western Blot of Parvalbumin and β -Actin bands, at ~12kDa and ~42kDa respectively, as indicated by molecular weight (kDa) ladder. Achieved by merging imaged bands with a colorimetric image of a prestained protein ladder (10-180kDa; ab116027). 65

ACKNOWLEDGEMENTS

When I reflect on this past year, I really think that this thesis would not be as good as it is today if not for the people that have been with me – I would like you all to know that. This unfortunately ruins my intentions of writing the rest of the page all about myself.

My greatest gratitude go to Dr. Martin Clark, who has had the pleasure to be my supervisor for technically two years if we include my undergraduate dissertation. I would be lying if I said that I haven't enjoyed being under your supervision and I am saddened that it is coming to an end. Thank you for all your dedication towards this project, thank you for your support and all the time that you invested in me and this project. Thank you for making this project possible in the first place, I will be forever grateful for this opportunity.

I would also like to thank Dr. Claire Mellor who has supported me through this project. This project would also not be possible without you. Thank you for the role as your lab demonstrator, it has been a genuine pleasure and a fantastic opportunity to work and learn from you.

Whether we have met four years ago and Wings Wednesdays with a game of pool has become our tradition, whether we met in our office, through the privilege of being housemates, at the weight section of the gym, or even if I once stole your seat at a conference, I appreciate that I had you all by my side. I want to thank all of you who have made me feel like at home in Preston. I cannot appreciate you all enough and I already miss you all. I wish you all the best of luck with all of your future endeavours. I would like to thank my friends from PABS, who have shared their invaluable knowledge and lab experience with me. I feel lucky to have had such great people and I think the impact of your mentorship is clear as day. Finally, I would like to thank my family. Dziękuję mojej rodzinie, chociaż nie jestem pewien, czy w pełni rozumieją pracę którą wykonuję w laboratorium. Mam szczęście, że mam tak kochającą i wspierającą rodzinę i jestem głęboko wdzięczny za waszą rolę w mojej podróży. Wasza ciągła obecność jest źródłem motywacji i inspiracji, dzięki którym mogę osiągać dalsze sukcesy.

Again, thank you to everyone who has made this journey with me.

ABBREVIATIONS

ASD	Autism spectrum disorder
BG	Basal ganglia
BTBR	BTBR T^+ <i>Itpr3^{fl}/J</i>
C57	C57L/J
chABC	Chondroitinase ABC
DLS	Dorsolateral striatum
DMS	Dorsomedial striatum
DS	Dorsal Striatum
E/I	Excitation to inhibition
FSI	Fast spiking interneuron
GABA	γ (gamma)-aminobutyric acid
GAD	Glutamic acid decarboxylase
IHC	Immunohistochemistry
IN	Interneuron
MSN	Medium spiny neuron
OFC	Orbitofrontal cortex
PV	Parvalbumin
PV+	Parvalbumin immunoreactive
RRBI	Restrictive and repetitive behaviour and interest
VPA	Valproic acid
VVA	Vicia villosa agglutinin
WB	Western blotting
WFA	Wisteria floribunda agglutinin

1.0 INTRODUCTION

Autism spectrum disorder (ASD) is a lifelong neurodevelopmental condition usually detected in early childhood (Courchesne et al., 2011). ASD is characterized by two core symptoms: (1) persistent deficits in social interaction and social communication, and (2) the presence of restricted, repetitive patterns of behaviours or interests (RRBIs; American Psychiatric Association, 2013). Stereotyped or repetitive motor movements, insistence on sameness, and highly restricted interests which are abnormal in intensity or focus are all symptoms of RRBIs which are among the most challenging facets of the disorder on an everyday basis (American Psychiatric Association, 2013). Currently, the underpinning cause of ASD is unknown. Although there is a genetic component, only a small percentage of cases is associated with known mutations, making ASD predominately idiopathic (Casanova et al., 2020; Meyza & Blanchard, 2017). Understanding the origin of RRBIs and the underlying neurobiology is required not only to our advancing models of the aetiology of ASD, but also to promoting the development of new interventions.

1.1 Striatal Dysfunction in ASD

Brain regions which have been implicated in ASD include the amygdala, orbitofrontal cortex (OFC), temporoparietal cortex, and insula (Weston, 2019). These regions have received much attention and have been well studied, particularly in relation the deficits observed in social communication and interaction. However, a region which has gained little attention yet has been proposed to underlie all of the core symptoms of ASD including RRBIs, is the basal ganglia (BG; Calderoni et al., 2014). The BG is a group of heavily interconnected subcortical nuclei proposed to be primarily responsible for motor behaviour as well as a range of other roles such as learning, executive functioning and emotions (Lanciego et al., 2012). This group of subcortical structures have been reported to be abnormal in ASD (Estes et al., 2011). In particular, dysfunction of the striatum, the main input nucleus of the BG has been postulated to underlie a range of autism-related behaviours, including repetitive motor behaviours, social and cognitive deficits, which are hallmarks of ASD (Fuccillo, 2016). Through the use of magnetic resonance imaging (MRI), studies have shown that individuals with ASD have an increased volume of the striatal nuclei compared to typically developing individuals (Langen et al., 2007; Sato et al., 2014). Furthermore, these volumetric changes positively correlated with repetitive behaviour scores (Hollander et al., 2005), which suggests of a causal relationship between volumetric alterations in the striatum and severity of RRBI symptoms.

Another MRI study showed that children with ASD had an increase in the growth rate of striatal brain structures compared to typically developing children, specifically in the caudate nucleus, where the growth rate was observed to be doubled. The faster growth rate was correlated with more severe repetitive behaviour (Langen et al., 2014; Kohls et al., 2014). This research proposes that RRBI may not be correlated with volume of the striatum nuclei per se but instead the rate of striatal growth. This still proposes convincing evidence that the striatal regions may be involved in the symptoms of RRBI in ASD, therefore it is rational to investigate this area further.

1.2 Dorsomedial and Dorsolateral Striatum Subregions

The striatum can be divided into ventral and dorsal striatum (DS), which subserve distinct roles in learning (Balleine et al., 2007). Flexible action selection and automatic action are some of the functions mediated by the DS (Balleine et al., 2007). The DS can be further subdivided into medial (DMS) and lateral (DLS) regions. In species which lack the internal capsule, such as rodents, DMS is roughly analogous to the caudate nucleus, while the DLS corresponds to the putamen (Lovinger & Mathur, 2016). While this division is not clear in mice, several lines of analysis suggest that rodent DMS and DLS exhibit similarities to both the human caudate nucleus and putamen. For example, such regions possess similar connectivity, with the DMS and the caudate nucleus both receiving inputs from the association cortices (Voorn et al., 2004). While the inputs to both DLS and the putamen are from sensorimotor cortices (Voorn et al., 2004). Functionally the two subregions differ, while the DMS is a crucial region for the acquisition and expression of goal-directed learning and behaviour (Yin et al., 2005; 2006), the DLS in turn governs habitual behaviour and formation of habits (Yin et al., 2004; 2006). Goal-directed behaviour is described as choosing actions depending on what consequences they have in a particular context (Zwosta et al., 2015). Goal-directed behaviour is distinguished by a high requirement for attention, is highly dependent on current reward value, and exhibits responsive flexibility (Griffiths et al., 2014). On the other hand, habitual behaviour is guided by behavioural automaticity and is stimulus-driven (Lipton et al., 2019). Symptoms of RRBI may manifest from a surplus of habitual behaviour and/or lack of goal-directed behaviour, with research indicating the alterations may be particularly localised to the caudate nucleus, the DMS region (Langen et al., 2014; Kohls et al., 2014). With previous research showing that these regions show clear differences in the connectivity and functionality, this provides an evidence-based rationale to investigate the medial and lateral

regions of the DS individually, which may be insightful to establishing the underpinning symptoms of ASD and in particular those associated with RRBI

1.3 Excitation and Inhibition Balance

An emerging theory holds that a disequilibrium between glutamatergic and GABAergic (γ -aminobutyric acidergic) signalling may underpin brain dysfunction and may result in symptoms of ASD (Rubenstein & Merzenich, 2003). The imbalance of these neurotransmitters, according to this framework, affects the ratio of excitation to inhibition (E/I), altering brain activity patterns and resulting in behavioural and cognitive impairments (Rubenstein & Merzenich, 2003). An imbalance in E/I may be caused by increased glutamatergic signalling or by a decrease in inhibition caused by a decrease in GABAergic signalling (Rubenstein & Merzenich, 2003). Dysfunction of the GABAergic system, which can be reflected by altered gamma band oscillations, has been particularly correlated with ASD (Yizhar et al., 2011). Research suggests that children and adolescents with ASD exhibit impaired gamma-band activity (Sun et al., 2012). These gamma-band oscillations have been found to be decreased compared to typically developing individuals (Snijders et al., 2013; Wilson et al., 2007), it is therefore an indication that individuals with ASD show altered E/I balance. Altered E/I balance has also been observed on a molecular level. Tissue analysis of post-mortem autistic patients, indicated that glutamic acid decarboxylase (GAD), both isoforms of GAD65 and GAD67, which are enzymes responsible for synthesis of glutamate to GABA, are reduced (~50%) in the parietal cortex and cerebellum (Fatemi et al., 2002; Yip et al., 2007). Therefore, this suggests that source of inhibition may be diminished in such regions of ASD individuals. In addition, levels of GABA_A and GABA_B receptors, which play an important role in synapse modulation and balance of E/I in the brain, have also been found to be reduced in individuals with ASD (Fatemi et al., 2009; Oblak et al., 2010). A decreased number of benzodiazepine binding sites in individuals with ASD further indicate alterations in the modulation of GABA_A receptors in the presence of GABA (Guptill et al., 2007). Relative to controls, ASD individuals have also been found with greater spine densities on pyramidal cells in the cortex, which provides structural support for connective changes (Hustler & Zhang, 2010). Furthermore, E/I imbalances are frequently observed in animal models of ASD, and their correction normalises key autistic-like phenotypes (Gogolla et al., 2014; Han et al., 2014; Lee et al., 2017). This forms compelling evidence of altered inhibitory system functioning, thus the altered ratio of E/I in the brain circuitry of those with ASD and in animal models of ASD. Suggesting E/I imbalances from alterations inhibitory signalling may contribute to the development of ASD.

1.4 Parvalbumin-Expressing Interneurons

Striatal neurons have been characterised on a number of levels. Structurally, these can be classed as either spiny projection neurons or aspiny interneurons (Kreitzer, 2009). Spiny projection neurons (SPNs), also known as medium spiny neurons (MSNs), constitute >95% of all striatal neurons in rodents and form the sole output to downstream BG nuclei (Tepper & Bolam, 2004). Aspiny interneurons make up <5% of all striatal neurons which can be divided anatomically into large cholinergic cells and medium-sized GABAergic cells (Kawaguchi et al. 1995). Medium-sized GABA releasing cells can further be divided into three categories: 1) parvalbumin-positive (PV+); 2) somatostatin-, neuropeptide Y-, and nitric oxide synthase-positive; and 3) calretinin-positive (Bennett & Bolam, 1993; Chesselet & Graybiel, 1986; Cowan et al., 1990; Vincent et al., 1983). While these constitute only a small fraction of the total striatal neuron number, these interneurons have a critical role in regulating output from the striatum. One of the most critical population of neurons involved in the inhibition of brain circuits, and which play a critical role in maintaining the E/I balance within neural circuits are interneurons (INs) that express the Ca²⁺ binding protein parvalbumin (PV). These inhibitory, GABAergic PV+ INs, alternatively known as fast-spiking interneurons (FSIs), possess low input resistance and high-amplitude rapid after-hyperpolarisation (Kawaguchi et al., 1987; Kawaguchi & Kubota, 1997). This combination of properties grants these INs the ability to fire rapid action potentials at a continuous high frequency of >50 Hz, which is considerably higher than the firing rates of MSNs (Nahar et al., 2021; Tepper & Bolam, 2004). Therefore, even synaptic potentials generated from a single PV+ IN is sufficiently powerful to alter the generation of action potentials in a large number of surrounding neurons simultaneously (Koós & Tepper, 1999). One distinctive feature of PV+ INs is their interconnectivity via dendritic gap junctions, which allow for direct transmission of electrical currents between coupled cells with a minor delay (Shigematsu et al., 2019). This property enables PV+ INs to fire synchronised action potentials, exerting even more powerful inhibitory control over neuronal circuits. By inhibiting a broad range of neurons simultaneously, such INs can synchronise the activity of other large populations of neurons and contribute to the generation of oscillatory network activity, such as gamma oscillations (30-80Hz; Lewis et al., 2012), important for various cognitive processes (Howard et al., 2003). Dysfunction and alterations in PV+ INs has been implicated in ASD, although these have been often in the cortical brain regions (Selten et al., 2018). Number of PV+ INs has previously been reported to be reduced in the prefrontal cortex of post-mortem individuals with ASD (Zikopoulos & Barbas, 2013; Hashemi et al., 2018; Ariza

et al., 2018). In addition, PVALB, the gene coding for PV, has been found to be the most strongly downregulated gene in individuals with ASD (Voineagu et al., 2011; Parikshak et al., 2013; Schwede et al., 2018). PV+ INs have also been found to be reduced in the neocortex across multiple ASD mouse models, sharing a similar PV-circuit disruption to that described in human ASD literature (Gogolla et al., 2009). Due to the powerful source inhibition that PV+ INs exhibit, even a minute disruption of such interneurons is likely to have a pronounced effect on the remainder of the BG circuitry and hence E/I balance (Ferguson & Gao, 2018). Intriguingly the distribution of such PV+ INs in the striatum is not uniform (Kita et al., 1990; Lee et al., 2012). There is an increasing gradient of such INs in the dorsal compared to ventral striatum but interestingly PV+ INs are enriched in the lateral striatum and much less evident in the medial striatum (Kita et al., 1990; Lee et al., 2012), suggesting that this gradient may exist due to the fact that the DMS and DLS regions govern different behaviours. Indeed, PV+ INs have been shown to critically play a role in habitual behaviour (Lee et al., 2017; O'Hare et al., 2017), therefore it is plausible that they may also contribute to symptoms of RRBI.

1.5 Loss of Pvalb Interneurons or Reduced PV Expression?

Perineuronal nets (PNNs) are extracellular matrix structures implicated in regulation of interneuronal activity and plasticity which surround primarily PV+ INs (Dityatev et al., 2007; Härtig et al., 1999). These structures can be detected based on the lectin-binding capacity of their glycan components with lectins such as *Vicia villosa agglutinin* (VVA) or *Wisteria floribunda agglutinin* (WFA) and therefore used as second marker for PV+ INs (Härtig et al., 2022). Upon incorporating PNNs as a second marker for PV+ INs, studies show that ASD mice models present with a reduction in the PV protein expression, rather than the commonly accepted conclusions of a loss of the neurons themselves, observed by a decreased number of PV+ cells without a reduction in the number of PNNs (Filice et al., 2016; Lauber et al., 2016; 2018). The class of interneurons defined by PV expression as well morphology, electrophysiological characteristics, and transcriptome profile is referred to as *Pvalb* neurons, regardless of PV expression level. The term PV+ neurons only to refer to neurons identified solely by PV IHC. Fewer PV+ neurons were observed in the striatum of ASD mice model *Shank3B^{-/-}* (-30%), *Cntnap2^{-/-}* (-30%), and in utero valproic acid (VPA)-treated (-15%) mice, with an unaltered number of PNNs accompanied by decreased PVALB mRNA and PV protein expression levels by ~50% (or by ~30% in VPA mice) suggests that the striatum is a hotspot for ASD-associated downregulation of PV (Filice et al., 2016; 2020; Lauber et al., 2016; 2018). Thus, the *Shank3B^{-/-}*, *Cntnap2^{-/-}*, and VPA mice models of ASD are characterised by

PV downregulation, not the loss of Pvalb neurons. Knockout of PV (PV^{-/-}) in mice results in completely absent expression of PV, yet brains of PV^{-/-} mice were found to harbour identical number of Pvalb neurons as wild-type (WT) mice, identified by an unaltered number of PNNs (Filice et al., 2016). Such PV^{-/-} mice display behavioural phenotypes with relevance to all core symptoms of ASD present in patients, nevertheless these mice also show signs of ASD-associated comorbidities, including reduced pain sensitivity and increased seizure susceptibility (Wöhr et al., 2015). Even when the mice underwent partial knockout of PV (PV^{+/-}) characterised by lower PV expression, reduced social interaction and communication were observed, indicating that even a reduction of PV levels is sufficient to elicit core ASD-like deficits (Wöhr et al., 2015). Similarly, when PV^{+/-} mice received an early postnatal administration of 17- β estradiol, which restored PV expression close to that of a WT mice (~90%), sociability deficits and repetitive behaviours were strongly ameliorated (Filice et al., 2018). These diverse lines of evidence suggest that PV downregulation may be a potential convergent endpoint for some types of ASD, not loss of Pvalb neurons. These alternative findings are of high significance, since the conclusions of reduced PV expression and conclusions of a loss of Pvalb neurons are likely to have opposing effects on E/I balance. Functionally, a loss of these inhibitory, Pvalb neurons is expected to result in a reduced inhibitory tone. A decrease in PV expression on the other hand results in enhanced paired-pulse facilitation, more excitable INs, which also fire more regularly, therefore enhancing inhibition (Caillard et al., 2000; Orduz et al., 2013). Still, PV downregulation as a potential convergent endpoint in ASD mice models has only been demonstrated in transgenic models and one environmentally insulted ASD model (Filice et al., 2016; Lauber et al., 2016; 2018). It is therefore not conclusive that such alterations occur across other stains, in particular idiopathic. Therefore, this provides a rationale for using an idiopathic mice model of ASD. Investigating for PV downregulation in BTBR mice would bridge the findings from that of transgenic and environmental models of ASD and aid in understanding the aetiology of ASD, which is predominantly idiopathic in nature, providing an even greater rationale for an investigation of the BTBR mouse.

1.6 Idiopathic Mouse Model of ASD

The study of ASD has proven to be a challenge due to its complex aetiology and vast heterogeneity among those affected, with only the behavioural phenotype in common. In order to better understand the underlying mechanism and develop interventions, research has begun to rely on animal models that exhibit behavioural and neuroanatomical characteristics

analogous to those observed in human individuals with ASD (Crawley, 2012). The most prevalent mice models which have been used to elucidate the aetiology of ASD have been genetically modified, transgenic mice models (Filice et al., 2016; Lauber et al., 2016; 2018), which have been indispensable in understanding ASD but despite great efforts, the majority of cases the genetic cause remains elusive. It is therefore essential to investigate models of idiopathic autism. A particularly strong candidate strain of idiopathic mice models is the BTBR T⁺ Itpr3^{tf}/J mouse (BTBR), which has been validated as a model of ASD in 2008 (McFarlane et al., 2008). The BTBR mice exhibit robust and consistent behavioural phenotypes that closely resemble the two core symptoms of ASD as defined in the DSM-5 (McFarlane et al., 2008; Moy et al., 2007). They demonstrate reduced social approach, reduced ultrasonic vocalisations, and low reciprocal social interactions as compared with controls, indicating impairments in social interaction and communication (Bolivar et al., 2007; Moy et al., 2007; Scattoni et al., 2011). Compared to control mice, BTBR mice also display elevated repetitive grooming, increased marble burying, and impairments in probabilistic reversal learning (a measure of cognitive flexibility) indicating that BTBR display aspects of RRBIs, including repetitive, stereotyped behaviour, and insistence on sameness (Amodeo et al., 2012; 2019; Moy et al., 2007). Notably, the idiopathic nature of the BTBR mice aligns with the reality of the majority of ASD cases in humans. The rationale for utilising the BTBR mouse model is to explore underlying mechanisms of ASD without the confounding factors associated with known mutations or specific genetic backgrounds. This allows for a broader investigation of potential aetiological factors that may contribute to the development of ASD leading to a more comprehensive understanding of the disorder and possibly uncover a biomarker which may be used to establish for early interventions to improve the lives of individuals with ASD.

1.7 Sex Differences in ASD and BTBR mice

A high male bias in ASD prevalence has been reported with remarkable consistency, with on average males being affected up to four times more than females (Baxter et al., 2015; Maenner et al., 2021). The persistence of this observation strongly suggests the presence of sex-specific biological factors playing a key role in the aetiology of ASD (Schaafsma & Pfaff, 2014; Werling & Geschwind, 2013). However, the underlying mechanism that contributes to the predominance of males among people with ASDs is yet to be definitively identified. Some research proposes that the male-to-female prevalence ratio may be closer to 3:1, with a diagnostic gender bias towards males meaning that females who meet the criteria for ASD are less likely to receive a clinical diagnosis (Loomes et al., 2017). Sex differences that emerge

when each core symptom of ASD is considered individually may account for this. Whilst males with a diagnosis of ASD are reported to show greater externalising and pro-social problems, (Mandy et al., 2012) females with ASD are reported with higher internalising symptoms, such as depression and anxiety (Solomon et al., 2012). Particularly, the higher frequency of RRBIs in males than females with ASD (Hattier et al., 2011; Szatmari et al., 2012), is representative of the sex differences observed in the idiopathic mouse model BTBR behavioural phenotype. (Amodeo et al., 2019; Schwartz et al., 2013). Although less consistently, male BTBR mice have also been suggested to show lower sociability than female counterparts (Amodeo et al., 2019; Defensor et al., 2011), meaning that such strain may be used to investigate sex-specific behaviours of ASD but crucially attempts can be made to investigate sex differences in the aetiology in BTBR mice which may predispose ASD-like symptoms.

1.8 Experimental Aims

The literature which proposes PV downregulation over a loss of Pvalb neurons in ASD mice models is becoming increasingly convincing. Ultimately, these two alternative conclusions have important implications as they are expected to result in opposing effects on E/I balance. The aim of this study was to utilise IHC and Western Blotting techniques to investigate whether BTBR, an idiopathic mice model of ASD, also presents with a decreased expression of the Ca²⁺ binding protein PV. This investigation would allow us to assess whether PV downregulation is also a convergent endpoint for idiopathic mice models of ASD, which would make a great contribution to our understanding of human ASD aetiology since investigation of parvalbumin downregulation has only been demonstrated in transgenic and environmental mice models of ASD. In this current study, the focus was on whether the alterations observed may be liable for the symptoms of RRBIs that are present in ASD, and of which BTBR mice exhibit in excess. Regulation of executive functions, action selection, and motor control are just some of the functions of the striatum (Balleine et al., 2007), with research strongly postulating that striatal dysfunction may underlie the symptoms of RRBIs observed in ASD (Fuccillo, 2016). Furthermore, the striatal regions have consistently shown to be a hotspot region for the downregulation of PV in previously investigated ASD mice models (Filice et al., 2016; Lauber et al., 2016; 2018). Therefore, this current study similarly aimed to investigate for these alterations, focusing on the dorsal striatum. The second aim of this study was to investigate subregional differences between the DMS and DLS regions, since functionally, the two regions contribute to two distinctive instrumental learning processes (Balleine et al., 2009).

While the DMS is largely involved in goal-directed behaviour (Yin et al., 2005; 2006), the DLS is involved in habit formation and behavioural flexibility (Yin et al., 2004). From this one can speculate that RRBI may underlie alterations in the two regions differently, or only one region may be observed with alterations. The third and last aim was to investigate sex differences in BTBR mice. This is of high importance because male BTBR mice exhibit higher rates of RRBI than female BTBR mice, which express comparable rates to that of control mice (Amodeo et al., 2019). Since BTBR female mice do not display equal RRBI profiles expressed by male counterparts, it may be suspected that aetiology may also differ, yet this has been overlooked by research which investigate predominantly male mice. Although highly speculative, if differences are observed between the sexes, extrapolations can be made that such differences may be the underlying mechanism of RRBI symptoms in ASD since both sexes show similar deficits in social communication and interaction, the other core symptom of human ASD.

1.9 Hypotheses

1. BTBR mice will have a significantly lower density of PV+ cells than C57 mice in the dorsal striatum.
2. There will be no significant difference in the density of VVA+ cells between BTBR and C57 mice in the dorsal striatum.
3. BTBR mice will have a significantly lower percentage of VVA+ cells with PV expression than C57 mice in the dorsal striatum.
4. BTBR mice will have a significantly higher percentage of PV+ cells surrounded by VVA than C57 mice in the dorsal striatum.
5. C57 mice will have a higher density of PV+ cells in the DLS than in the DMS.
6. C57 mice will have a higher density of VVA+ cells in the DLS than in the DMS.
7. C57 mice will have a higher percentage of VVA+ cells with PV expression in the DLS than in the DMS.
8. C57 mice will have a higher percentage of PV+ surrounded by VVA in the DLS than in the DMS.
9. BTBR mice will have a significantly lower density of PV+ cells than C57 mice in the DMS
10. There will be no significant difference in the density of VVA+ cells between BTBR and C57 mice in the DMS.
11. BTBR mice will have a significantly lower percentage of VVA+ cells with PV expression than C57 mice in the DMS
12. BTBR will have a significantly higher percentage of PV+ cells surrounded by VVA than C57 mice in the DMS.
13. Male BTBR mice will have a higher density of PV+ cells than female BTBR mice in the DLS
14. Male BTBR mice will have a lower percentage of PV+ cells surrounded by VVA than female BTBR mice in the DMS
15. Male BTBR mice will have a lower percentage of PV+ cells surrounded by VVA than female BTBR mice in the DMS
16. PV expression levels will be significantly lower in the striatum of BTBR mice compared to C57 mice.

2.0 MATERIALS AND METHODS

2.1 Animals

All mice brains were purchased from The Jackson Laboratory (Bar Harbor, Maine, USA). All brains were harvested from 8-week-old mice. Five right hemispheres from male BTBR T⁺ Ipr3^{tf}/J mice (BTBR, strain no. 002282) and five right hemispheres from male C57L/J mice (C57, strain no. 000668) were harvested and snap frozen at The Jackson Laboratory, later stored at -80°C until dissection and used for western blotting analysis.

For fluorescent IHC, 10 left hemispheres from BTBR mice (5 male & 5 female) and 10 left hemispheres from C57 mice (5 male & 5 female) were perfusion-fixed then fixed with 4% paraformaldehyde for additional 24 to 48 h. The use of this secondary tissue has been ethically approved by AWERB 19 04.

2.2 Tissue Dissection

Dissections were carried out on a chilled glass plate, placed on ice. Left and right hemispheres were separated along the midline, after which only the right hemisphere was further micro-dissected. First, the cerebellum was cut off along the brain stem. The genu of the corpus callosum, fornix and anterior commissure were located (see **Figure 1A**). With the use of a razor blade a coronal incision was made anterior of the genu of the corpus callosum (at approx. 1.10mm Bregma), yielding tissue containing prefrontal cortex. A second coronal incision was made posterior of the anterior commissure and fornix (at approx. -0.10mm Bregma), at which the cut yielded a disk, which contained the striatum encapsulated by the corpus callosum and septal regions. The cortex was separated from the striatum along the corpus callosum, the septum was also separated away by gently peeling away medial regions of the lateral ventricle from the striatum, striatum was then collected (see **Figure 1B**). The cortex was peeled away from the midline to expose the hippocampus, after which the darker in colour hippocampus was dissected away from the cortex using a scalpel. At this point, the cortex would be pulled away from the midbrain structures to also be collected. All tissue samples were placed into 1.5ml Eppendorf tubes and stored at -80°C. For a demonstration of the full dissection procedure see **Appendix A**.

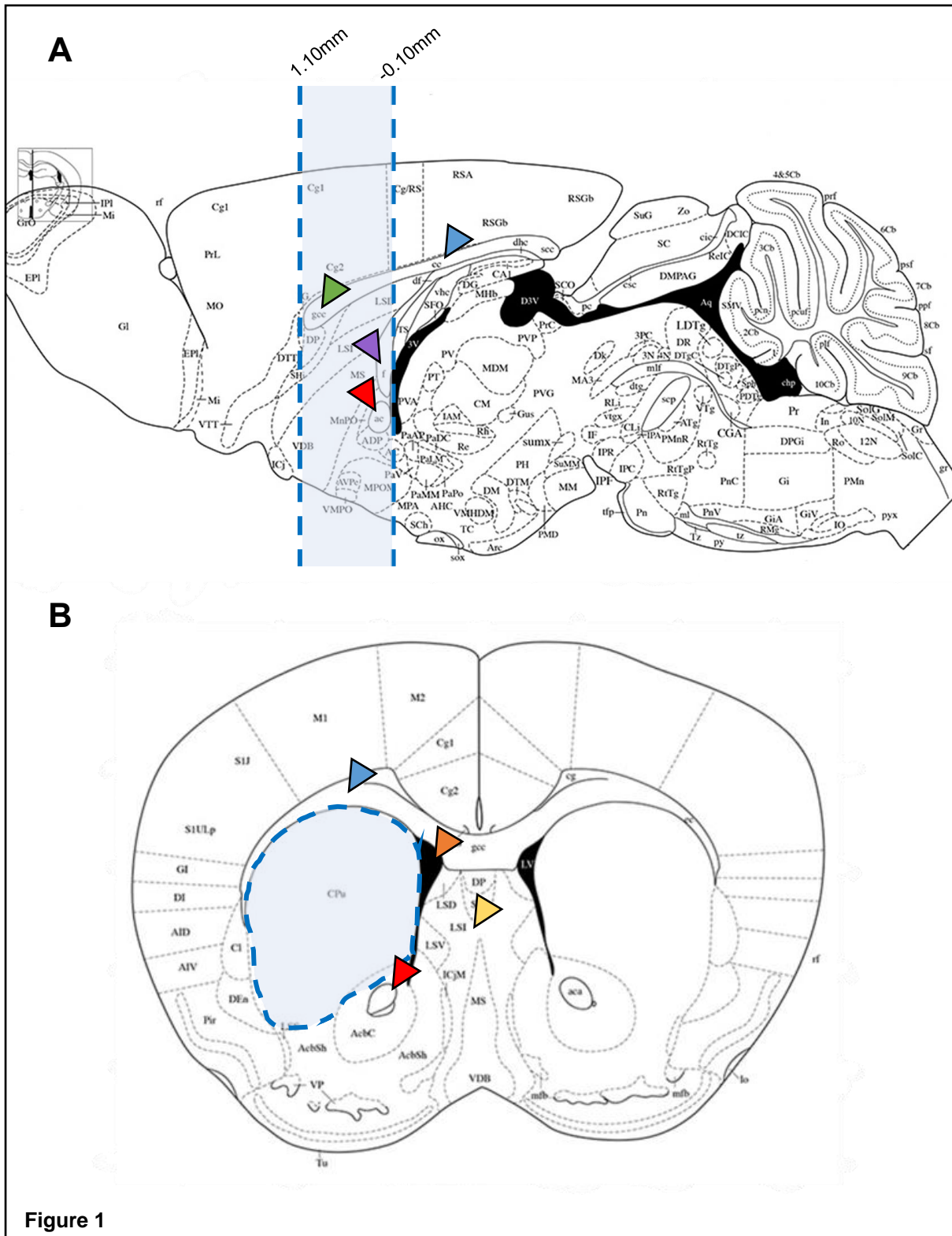


Figure 1 | Mouse Brain Atlas adapted from Franklin and Paxinos (2007) with visual representation of striatal dissection procedure. (A) Sagittal section of mouse brain at 0.12mm lateral. Incisions made posterior of the genu of the corpus callosum (approx. 1.10mm bregma) and posterior of the anterior commissure and fornix (approx. -0.10mm bregma), yielded a disk which contained the striatum (shaded light blue). (B) Coronal section of mouse brain at 1.10mm bregma. Striatum (shaded light blue region) was dissected away from the cortex along the corpus callosum and septum along the lateral ventricle. Triangles indicate the corpus callosum (blue), genu of the corpus callosum (green), fornix (purple), anterior commissure (red), septal regions (yellow), and lateral ventricle (orange).

2.3 Tissue Preparation and Immunohistochemistry

After dissecting the post-fixed brains along the midline, the left hemispheres were cryopreserved in increasing concentrations of sucrose-PBS, 15% and 30% respectively, at 4°C. The hemispheres were then embedded in an optimal cutting temperature (OCT) medium with the orientation optimal for coronal sectioning and allowed to freeze. The frozen OCT-embedded hemisphere was adhered to the cryostat platform with the use of room temperature OCT and placed into the cryostat chamber to freeze. Hemispheres were placed into the cutting position and the angle of the blade adjusted. Coronal sections were cut rostral-caudally into 20µm sections using the cryostat.

Free-floating sections were first incubated with PBS 0.01M plus 0.3% Triton X-100 (TX) with 5% normal goat serum (NGS) and 2.5% bovine serum albumin (BSA) for 30 min at room temperature (RT), then washed three times with PBS 0.01M for 10 minutes each. Incubated with anti-PV Guinea pig antibody (Synaptic Systems, Cat No. 195004) at a dilution 1:2000 and *Vicia villosa agglutinin* (Vector labs, Biotinylated - B-1235-2) at a dilution 1:200 in PBS 0.01M plus TX 0.3%, 5% NGS and 2.5% BSA overnight at RT. Sections were washed twice with PBS 0.01M and incubated protected from light at RT with Alexa 488 goat anti-Guinea pig (1:500 dilution, abcam, Ab150185) and Streptavidin, Texas Red (1:200 dilution, Vector Labs, SA-5006-1) in PBS 0.01M plus TX 0.3%, 5% NGS and 2.5% BSA for 2 h. The sections were washed two more times with PBS 0.01M for 10 min each before mounted onto a slide and left to dry at RT for 15-30 min in the dark. The sections were cover slipped with Vectashield mounting medium containing DAPI. Sections were stored at 4°C until visualisation.

2.3 Tissue Selection

In order to obtain sections with the striatum, Franklin and Paxinos (2007) mouse brain atlas was used to identify and select the coronal slices between the bregma 1.10mm and -0.10mm. The striatum, depicted as the 'CPu' can be observed to be present between such bregma ranges (**Figure 2A & B**). Slices were identified based on the appearance of the corpus callosum, lateral ventricle and anterior commissure. In C57 mice, at bregma 1.10mm, the corpus callosum began to merge clearly with the medial eminence. This observation was maintained as a criteria through to bregma -0.10mm. In BTBR mice, there was no merging with the medial eminence since they lack the corpus callosum (Stephenson et al., 2011)

however the striatum was capsuled by white matter tracts from the corpus callosum to a degree which was comparative to that of a bregma in C57 mice. The lateral ventricle was present, although to a less clear extent in BTBR mice, and slices were selected up until the merge with the dorsal third ventricle. The anterior commissure at bregma 1.10mm was clearly observed in both C57 and BTBR mice. Slices were obtained until the anterior commissure begins to finish meeting the midline at bregma -0.10mm.

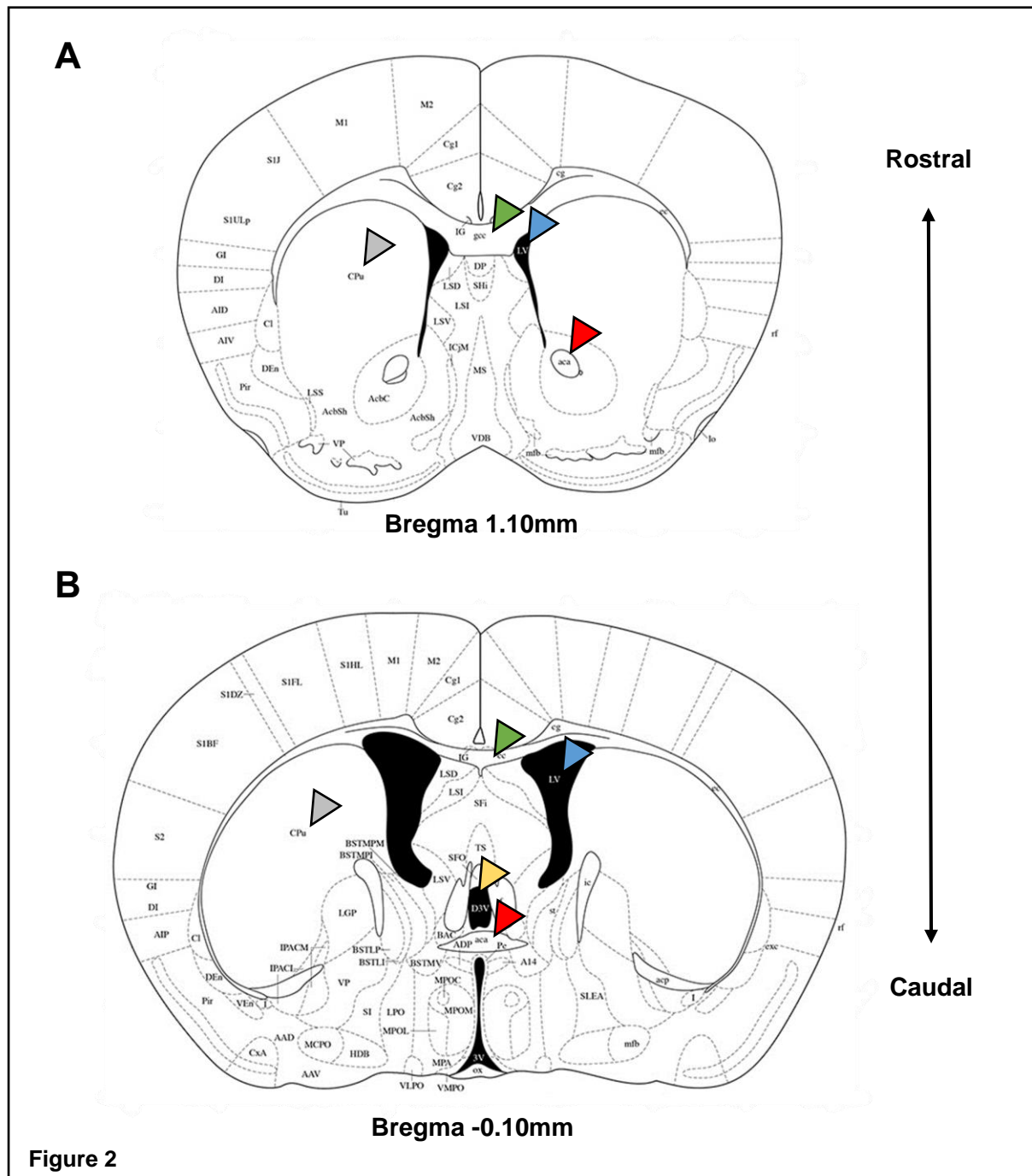


Figure 2 | Mouse brain atlas adapted from Franklin and Paxinos (2007), indicating regions used to distinguish presence of the striatum. (A) Coronal section of mouse brain at 1.10mm bregma. (B) Coronal section of a mouse brain at -0.10mm bregma. Triangles indicate the striatum (grey), corpus

callosum (green), lateral ventricle (blue), dorsal third ventricle (yellow), and anterior commissure (red).

2.4 Image Acquisition & Region of Interest Selection

PV+ and VVA+ cells were visualised using a Zeiss Cell Observer inverted microscope with a motorised x-y stage and coupled to an AxioCam camera. The left hemispheres were imaged using a tile function and a 20x dry lens. An image with a height: 1500 μ m and width: 2500 μ m, captured the DS, corpus callosum, and lateral ventricle. See **Appendix B** for details of used filter sets and their corresponding excitation and emission wavelength spectrums.

Fiji software (ImageJ 2.9.0) was used to determine the ROIs (DMS and DLS). First, a vertical 1mm measurement from underneath the corpus callosum was taken. From the bottom of that measurement, a horizontal measurement from the edge of the lateral ventricle to the arch of the corpus callosum established the width of the DS (see **Figure 3A**). The width determined the diameter of the ROIs. Each slice had the width of the DS determined and ROI calculated to possess a diameter which is 35% of the DS width. The DMS ROI is then positioned laterally to the lateral ventricle and inferior to the corpus callosum. The DLS was placed further laterally to the DMS ROI ensuring that the two regions do not overlap, with close proximity to the corpus callosum (see **Figure 3B**).

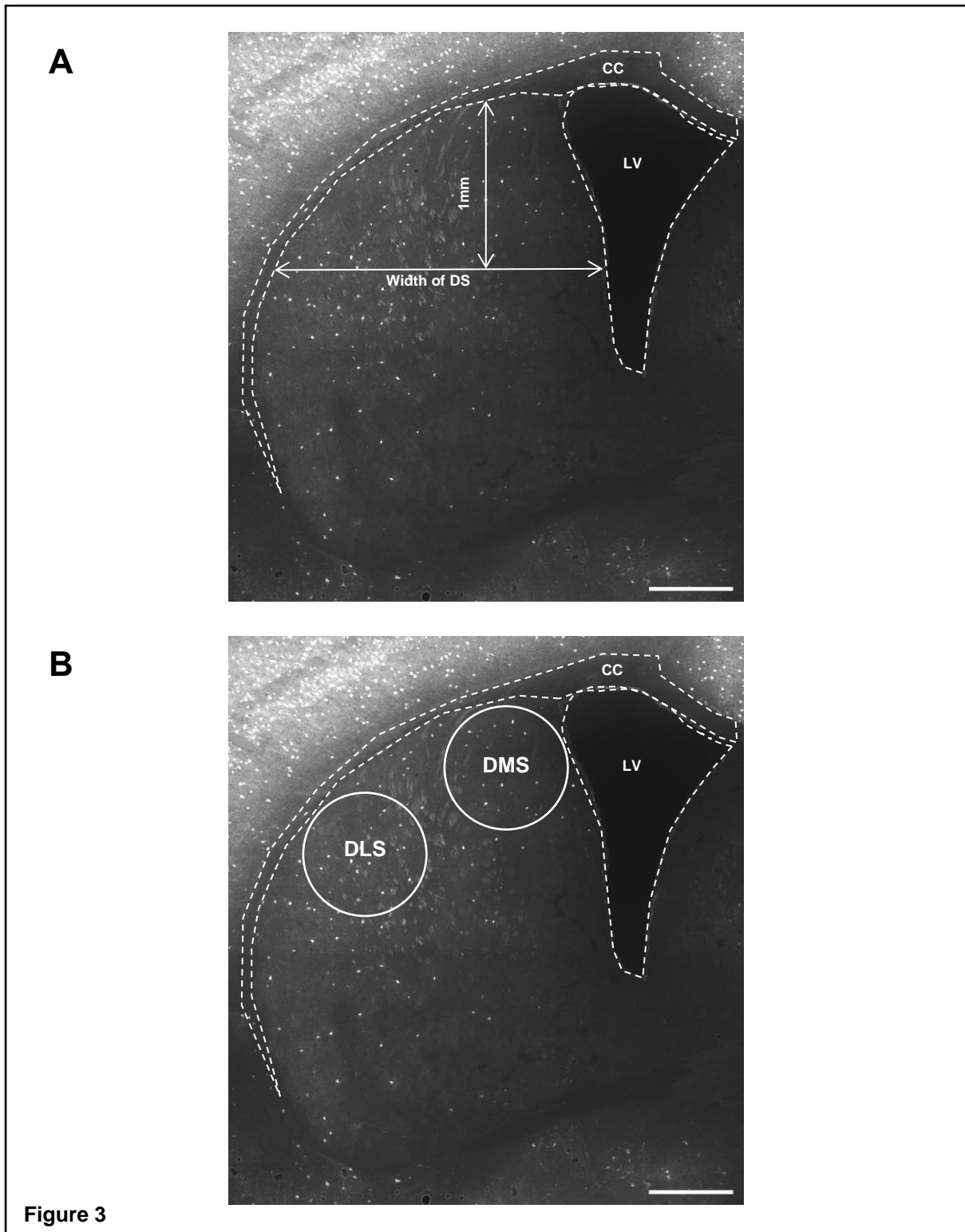


Figure 3 | Representative PV immunofluorescence images from the striatum of a C57 mouse, visualising the selection process of ROIs (DMS and DLS). (A) Vertical 1mm measurement from the most dorsal region of the striatum was taken (under the corpus callosum; CC), after which a horizontal measurement captured the width of the dorsal striatum (DS) from the beginning of the lateral ventricle (LV) to the edge of the CC. (B) The diameter of the ROIs were determined by 35% of the DS width. DMS ROIs were determined, with close proximity, lateral to the LV and inferior to the CC. DLS ROIs were determined laterally to that of the DMS, without overlap, and close proximity to the CC. Scale bar: 500µm.

2.5 Counting Criteria

PV+ and VVA+ cells were counted independently and according to the following predefined criteria (1) presence of a DAPI stained nucleus; (2) well defined and roundish PNN for VVA+ cells, and (3) PV staining surrounding the DAPI stained nucleus for PV+ cells, examples are shown in **Figure 4**. Additionally, to meeting the criteria as a cell, these must also be present within or on the border of the ROI.

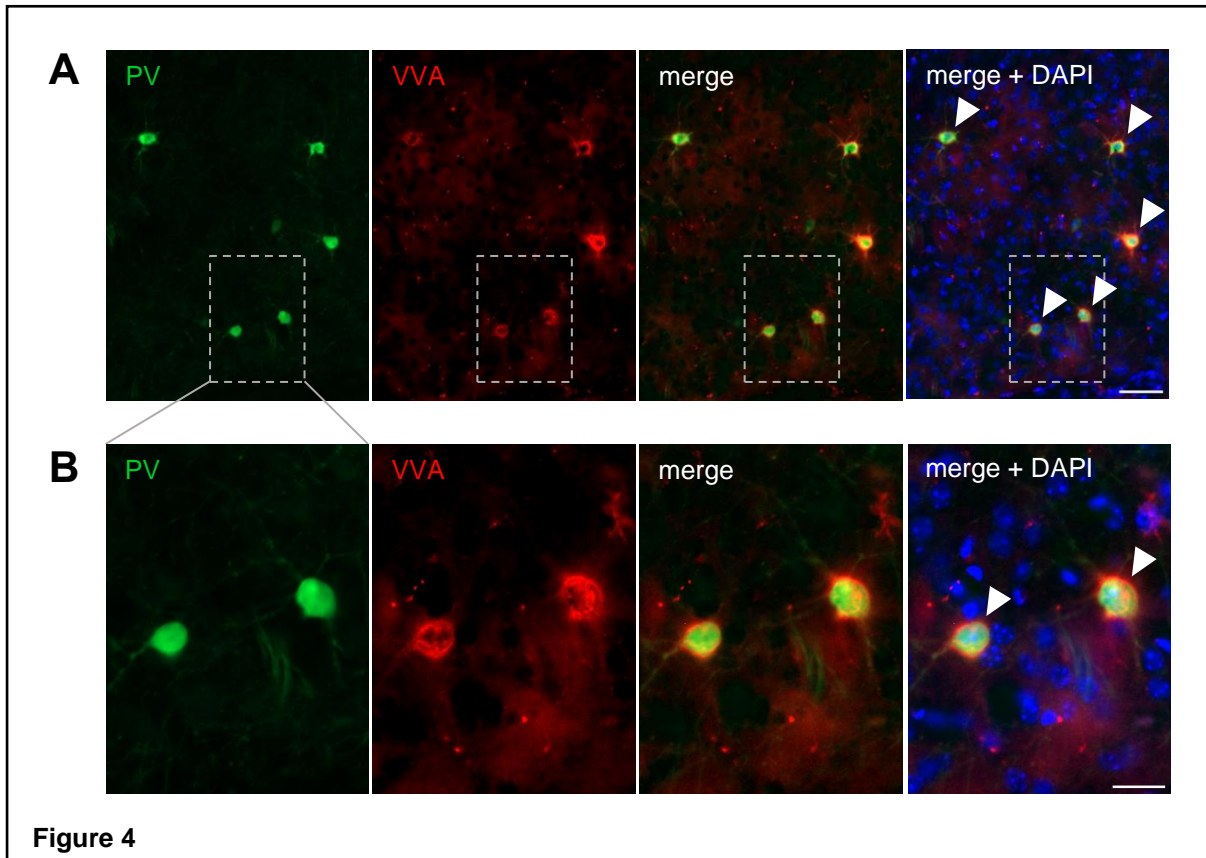


Figure 4 | Representative images of PV+ cells, VVA+ cells, and PV+VVA+ co-localisation from mouse dorsal striatum (DS), matching the predefined criteria. (A) PV+ cells (green), VVA+ cells (red), merged images showing PV and VVA overlapping in the DS of a C57 mouse. Slices were counterstained with DAPI (blue). (B) Enlarged images of the boxes outlined in A. White triangles point at in focus PV+VVA+ double positive cells, with a clearly stained DAPI nucleus. Scale bar: (A) 50 μ m; (B) 20 μ m.

2.6 Cell Density & Colocalisation Percentage

Cell counts of PV+ and VVA+ cells were converted to cell densities. Area of the ROIs were determined with known diameter using the equation:

$$A = \frac{1}{4}\pi d^2$$

Where A is area (mm²), and d is diameter (mm). Cell counts were divided by the area of their respective ROI to obtain density (cells/mm²). % of PV+ cells surrounded by VVA was obtained by dividing the number of PV+VVA+ colocalised cells by the number of PV+ cells and multiplying by 100 to obtain a percentage. % of VVA+ cells with PV expression was obtained by dividing the number of PV+VVA+ colocalised cells by the number of VVA+ cells and multiplied by 100 to obtain a percentage.

2.7 Protein Lysate Preparation

400µl of homogenisation buffer [10mM Tris pH 7.4, 100mM NaCl, 1mM Ethylenediaminetetraacetic acid (EDTA), One tablet of protease inhibitors per 10ml of buffer] was added to previously dissected striatal tissue. Tissue was homogenised manually with a mini pestle for 10 sec intervals followed by resting for 10 sec on ice and repeated for 5 minutes. Considering the concentrations of reagents in the homogenisation buffer, a series of reagents were added to yield final concentrations of RIPA lysis buffer [50mM Tris pH 7.5, 150mM NaCl, 5mM EDTA, 1% sodium dodecyl sulfate (SDS), 1% Triton X-100, 0.5% Sodium deoxycholate]. The lysate was rotated for 30 minutes on the Stuart Rotator at 40 rpm at 4°C, followed by vortexing the lysate for 5 sec then resting on ice for 5 sec, repeated for 1 min. Lysate was centrifuged at 14,000 rpm for 10 min at 4°C after which the supernatant was collected into a clean 1.5ml microcentrifuge tube, centrifuged once more at 14,000 rpm (20,817 rcf; Eppendorf Centrifuge 5430R) for 10 min at 4°C. Supernatant was collected and stored at -80°C.

2.8 BCA Protein Assay

In order to quantify total amount of proteins in lysates the Pierce Bicinchoninic Acid (BCA) protein assay was carried out. Using the Radioimmunoprecipitation assay (RIPA) buffer and Bovine Serum Albumin (BSA) 2mg/ml, serial dilutions of BSA were prepared ranging from 0mg/ml (RIPA only) to 2mg/mL. 20µl serial dilutions of BSA and of each of the 10

lysates were added to the wells of a transparent flat bottom 96 well plate. Working reagent was achieved by combining reagent A and B (50:1). 200µl of working reagent was pipetted into the wells with the lysate and BSA dilutions. Plate was covered in foil, placed on a plate shaker for 5 min and then incubated for 30 min at 37°C. Absorbance measurements were taken using a Tecan Spark plate reader at a wavelength of 562nm. A standard curve graph of BSA serial dilutions was produced (**Figure 5**), which was used to calculate the unknown concentrations of the lysate samples and determine the volume of each lysate required to obtain 10µg of proteins (**Appendix C**).

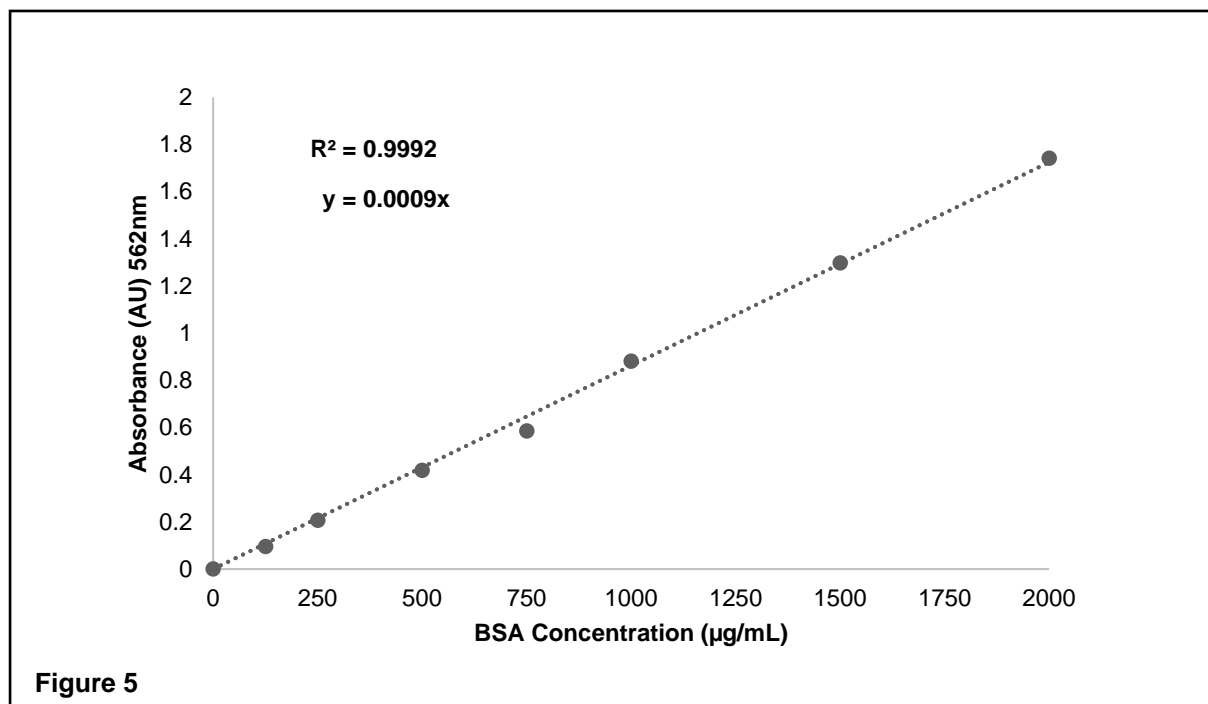


Figure 5 | *BCA assay standard curve of Bovine Serum Albumin (BSA) concentration (µg/µL) versus absorbance (AU). Absorbance measurements taken at a wavelength of 562nm.*

2.9 SDS-PAGE Gel Electrophoresis

10µg of proteins from each lysate was added to an equal volume of 2X Laemmli buffer [125mM Tris-HCl pH 6.8, 4% SDS, 20% Glycerol, 0.02% Bromophenol blue, 10% 2-mercaptoethanol (added immediately before use)]. Samples were heated at 95°C for 5 min at 300 rpm using an Eppendorf Thermomixer C. Reduced and denatured proteins were loaded into the wells of a 12% TGX (Tris-Glycine eXtended) gel and ran by filling the tank with the running buffer (BioRad, Tris/Glycine/SDS) at 50V for 15 minutes, or until the dye front has

passed the wells of the gel, after which the voltage was turned up to 100V and ran until dye front was almost reaching the bottom of the gel (~1 h).

2.10 Wet Transfer

Nitrocellulose membrane was cut to the appropriate dimensions (8.5 x 6.5cm) and submerged for 10 mins in Towbin transfer buffer [25mM Tris pH 8.3, 192mM Glycine, 20% Methanol]. The transfer cassette was assembled as appropriate using 2 sponges and 2 filter papers, ensuring that the gel is placed closer to the cathode (-) electrode side (black) and the membrane closer to the anode (+) electrode side (red), then inserted into the transfer tank with Towbin transfer buffer and an ice block. Transfer was run at 150mA for 1 h at 4°C.

2.11 Western blotting

After the transfer, the membranes were washed 3 times for 5 min with TBS with 0.1% Tween (TBS-T). The membranes were initially blocked at RT for 1 h in 5% non-fat milk TBS-T, followed by incubation with guinea pig anti-PV primary antibody (Synaptic Systems, Cat no: 195004) diluted 1:2000 in TBST and 2% non-fat milk with vertical agitation at RT for 1 h. Membranes were rinsed 3 times for 5 mins with TBS-T before being incubated for 1 h at RT with anti-guinea pig IgG HRP-conjugated secondary antibody (Proteintech, Cat no: SA00001-12) diluted 1:10,000 in TBST and 2% non-fat milk. Membranes were washed 3 times for 5 min with TBS-T before development of PV bands using the enhanced chemiluminescence (ECL) detection method.

In order to obtain β -actin bands as loading controls, similar steps were repeated. Membranes were washed 3 times for 5 min with TBS with 0.1% Tween (TBS-T). The membranes were re-blocked at RT for 1 h in 5% non-fat milk TBS-T, followed by incubation with rabbit anti- β -actin primary antibody (Proteintech, Cat no: 20536-1-AP) diluted 1:10,000 in TBST and 2% non-fat milk with vertical agitation at RT for 1 h. Membranes were rinsed 3 times for 5 mins with TBS-T before being incubated for 1 h at RT with anti-rabbit IgG HRP-conjugated secondary antibody (Proteintech, Cat no: SA00001-2) diluted 1:10,000 in TBST and 2% non-fat milk. Membranes were washed 3 times for 5 min with TBS-T before development of β -actin bands using ECL detection method.

SuperSignal™ West Pico PLUS Chemiluminescent Substrate (ThermoFisher Scientific, Cat no. 34580) was used for the detection method. This involved mixing reagent 1 (Stable Peroxide) and reagent 2 (Luminol/Enhancer) into a 1:1 ratio for 1 minute. Then

incubating the membrane in the solution for another 4 min. The membrane was imaged using BioRad Chemidoc.

2.12 Blot Quantification

To quantify the levels of PV from Western Blot images, ImageLab software (version 6.1, Bio-Rad Laboratories) was used to measure the intensity of PV bands and background noise for each lane. The background intensity was then subtracted from its corresponding lane with PV bands to reach an adjusted intensity of PV. The same procedure was repeated for the loading control, β -Actin. The normalisation factor was determined by dividing each lane's adjusted β -Actin intensity by the highest adjusted β -Actin intensity on that membrane. To obtain a normalised experimental signal, the intensity of each PV bands were divided by their corresponding lane normalisation factor. An average of PV normalised signal (100%) from C57 tissue was calculated for each membrane. Then individual samples were converted to percentage of C57 tissue by dividing by the average PV normalised signal (100%) from C57 tissue. An average was obtained from 3 separate experiments. PV levels are presented as a percentage of C57 tissue, where C57 tissue sample is defined as 100%.

2.13 Statistical Analysis

GraphPad Prism Software (version: 10.1.1, San Diego, USA) was used to analyse all data. IHC data were first checked for normal distribution by the Shapiro-Wilk test, then analysed with a Two-way ANOVA. Tukey's test was performed as a post hoc test. A one-tailed, unpaired t-test was used to compare PV protein levels between animal models. A p -value < 0.05 was considered statistically significant.

3.0 RESULTS

3.1 Immunohistochemistry - Dorsal Striatum

To begin, the results of the IHC analysis shows the population density of PV+ cells (see **Table 1**), the density of VVA+ cells (see **Table 2**), the percentage of VVA+ cells with PV expression (see **Table 3**), and percentage of PV+ cells surrounded by VVA (see **Table 4**) all of which are present in the DS in C57 and BTBR mice. This analysis investigated whether there were differences between BTBR mice and control, C57 mice at the level of the DS before investigating subregions.

Table 1 | Mean and standard deviation (SD) of PV+ cell density (cells/mm²) in the Dorsal Striatum of male and female, C57 and BTBR mice.

	PV+ Cell Density (cells/mm ²)		
	C57 (SD)	BTBR (SD)	Row Means (SD)
Male	26.64 (3.74)	22.60 (3.56)	24.62 (4.05)
Female	26.70 (2.00)	18.96 (2.38)	22.83 (4.57)
Column Means	26.67 (2.80)	20.78 (3.43)	

Table 2 | Mean and standard deviation (SD) of VVA+ cell density (cells/mm²) in the Dorsal Striatum of male and female, C57 and BTBR mice.

	VVA+ Cell Density (cells/mm ²)		
	C57 (SD)	BTBR (SD)	Row Means (SD)
Male	30.62 (4.28)	27.46 (4.02)	29.04 (4.25)
Female	28.94 (2.19)	28.48 (2.96)	28.71 (2.47)
Column Means	29.78 (3.32)	27.97 (3.38)	

Table 3 | Mean and standard deviation (SD) of Percentage of VVA+ cells with PV expression in the Dorsal Striatum of male and female, C57 and BTBR mice.

	% of VVA+ cells with PV expression		
	C57 (SD)	BTBR (SD)	Row Means (SD)
Male	64.86 (6.29)	56.54 (5.11)	60.70 (6.95)
Female	75.22 (5.18)	60.18 (3.97)	67.70 (9.04)
Column Means	70.04 (7.71)	58.36 (4.72)	

Table 4 | Mean and standard deviation (SD) of Percentage of PV+ cells surrounded by VVA in the Dorsal Striatum of male and female, C57 and BTBR mice.

	% of PV+ cells surrounded by VVA		
	C57 (SD)	BTBR (SD)	Row Means (SD)
Male	73.54 (6.48)	69.56 (6.81)	71.55 (6.61)
Female	80.52 (2.22)	90.58 (1.62)	85.55 (5.61)
Column Means	77.03 (5.86)	80.07 (12.02)	

A two-way ANOVA was performed to analyse the effects of animal model and sex on PV+ cell density in the DS. Simple main effects analysis showed that animal model did have a significant effect on the density of PV+ cells ($F_{(1,16)} = 19.07$, $p < .001$, **Figure 6A**). These results suggest that BTBR mice present with a ~22% decrease in PV+ cell density compared to control mice in the DS. Simple main effects analysis showed that sex did not have a statistically significant effect on the density of PV+ cells ($F_{(1,16)} = 1.76$, $p = .203$). A two-way ANOVA revealed that there was no statistically significant interaction between the effects of animal model and sex ($F_{(1,16)} = 1.88$, $p = .189$).

Post hoc testing using Tukey's multiple comparisons test indicated that the density of PV+ cells in the DS was significantly lower in female BTBR mice (18.96 ± 2.38 cells/mm²) than in female C57 mice (26.70 ± 2.00 cells/mm²; $p = .005$, **Figure 6E**). However, there was no significant difference between the density of PV+ cells in the DS of male BTBR mice (22.60 ± 3.56 cells/mm²) and male C57 mice (26.64 ± 3.74 cells/mm²; $p = .189$, **Figure 6E**). These results suggest that female BTBR mice have a ~29% decrease in PV+ cell density in the DS compared to female control mice. Compared to female controls, male BTBR mice also present with a decreased density of PV+ INs but such reduction is not significant.

A two-way ANOVA was performed to analyse the effects of animal model and sex on VVA+ cell density in the DS (**Figure 6B**). Simple main effects analysis showed that animal model did not have a statistically significant effect on the density of VVA+ cells ($F_{(1,16)} = 1.36$, $p = .260$, **Figure 6F**). Simple main effects analysis showed that sex did not have a statistically significant effect on the density of VVA+ cells ($F_{(1,16)} = 0.04$, $p = .834$). There was no statistically significant interaction between the effects of animal model and sex ($F_{(1,16)} = 0.76$, $p = .397$). These results suggest that the density of PNNs are unaltered between BTBR and control mice and between sexes in the DS.

A two-way ANOVA was performed to analyse the effects of animal model and sex on the percentage of VVA+ cells with PV expression in the DS. Simple main effects analysis showed that animal model did have a significant effect on the percentage of VVA+ cells with PV expression ($F(1,16) = 25.18, p < .001$, **Figure 6C**). These results suggest that, compared to controls, BTBR mice have ~12% less VVA+ cells with PV expression. Simple main effects analysis showed that sex also had a significant effect on the percentage of VVA+ cells with PV expression ($F(1,16) = 9.05, p = .008$), suggesting that female mice have higher percentage of VVA+ cells with PV expression than male counterparts. There was no statistically significant interaction between the effects of animal model and sex ($F(1,16) = 2.08, p = .168$).

Post hoc testing using Tukey's multiple comparisons test indicated that the percentage of VVA+ cells with PV expression in the DS was significantly lower in female BTBR mice ($60.18 \pm 3.97\%$) than in female C57 mice ($75.22 \pm 5.18\%$; $p = .002$, **Figure 6G**). The percentage of VVA+ cells with PV expression was also significantly lower in male C57 mice ($64.86 \pm 6.29\%$) than in female C57 mice ($75.22 \pm 5.18\%$; $p = .029$, **Figure 6G**). These results suggest that female BTBR mice have ~15% less VVA+ cells with PV expression, whilst male BTBR mice have ~10% less VVA+ cells with PV expression, which coincides with the decreased density of PV+ cells but unaltered density of VVA+ cells. Overall suggesting that BTBR mice, both male and female, show a decreased expression of PV in the DS, not a loss of Pvalb INs themselves.

A two-way ANOVA was performed to analyse the effects of animal model and sex on the percentage of PV+ cells surrounded by VVA in the DS. Simple main effects analysis showed that animal model did not have a significant effect on the percentage of PV+ cells surrounded by VVA ($F(1,16) = 1.92, p = .185$, **Figure 6D**). Simple main effects analysis showed that sex did have a significant effect on the percentage of PV+ cells surrounded by VVA ($F(1,16) = 40.67, p < .001$). These results suggest that female mice have ~14% more PV+ cells surrounded by VVA in the DS. There was a statistically significant interaction between the effects of animal model and sex ($F(1,16) = 10.23, p = .006$).

Post hoc testing using Tukey's multiple comparisons test indicated that the percentage of PV+ cells surrounded by VVA in the DS was significantly higher in female BTBR mice ($90.58 \pm 1.62\%$) than in male BTBR mice ($69.56 \pm 6.81\%$; $p < .001$, **Figure 6H**). There was no significant difference observed between male and female C57 mice, suggesting that BTBR mice possess a sex-linked difference in colocalisation of PV+ cells with PNNs. The percentage of

PV+ cells surrounded by VVA was also significantly higher in female BTBR mice ($90.58 \pm 1.62\%$) than in female C57 mice ($80.52 \pm 2.22\%$; $p = .024$, **Figure 6H**). This in turn shows that female BTBR mice have ~10% more PV+ INs ensheathed by PNNs compared to control female counterparts.

In conclusion, we observe that at the level of the DS, BTBR mice present with a decreased expression of PV rather than a loss of Pvalb INs. We are able to conclude this from the reduced density of PV+ INs but an unaltered density of VVA+ cells, visualising PNNs. BTBR mice also show a reduced percentage of VVA+ cells with PV expression, therefore further supporting the results of this study that in fact BTBR present with a downregulation of PV. The percentage of PV+ cells surrounded by VVA seems to be unaltered in the DS of BTBR mice, however upon further investigation female BTBR mice were found to have colocalisation than male BTBR mice.

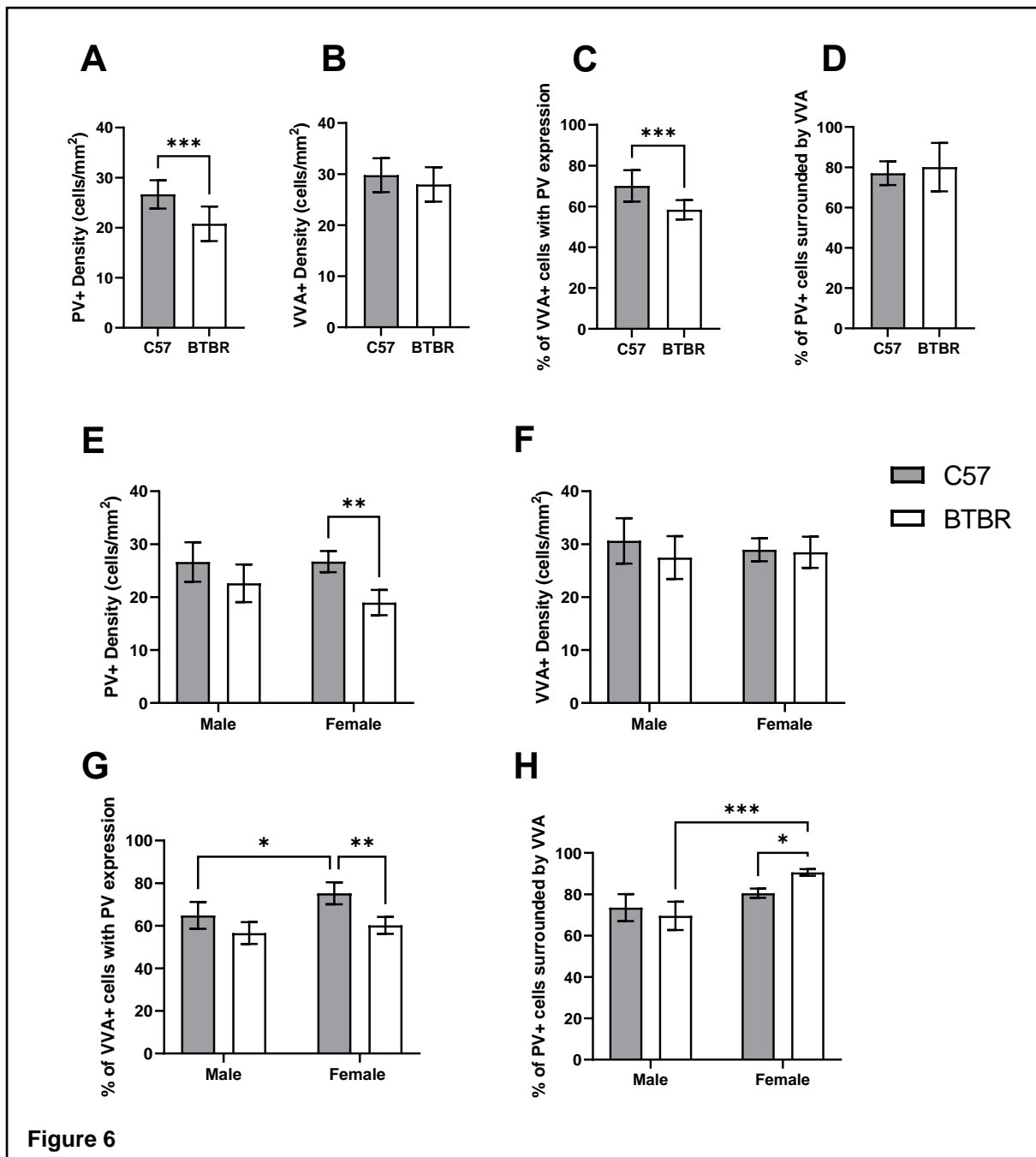


Figure 6 | Bar charts showing, irrespective of sex, mean (\pm SD) PV+ cell density (A), mean (\pm SD) VVA+ cell density (B), mean (\pm SD) percentage of VVA+ cells with PV expression (C) and mean (\pm SD) percentage of PV+ cells surrounded by VVA (D) in the Dorsal Striatum of C57 (grey) and BTBR (white) mice. (E-H) Bar charts show differences between male and female mice. Asterisks represent * $p \leq 0.05$, ** $p \leq 0.01$ and *** $p \leq 0.001$, respectively.

3.2 Subregional & Sex Differences

Focusing on the subregional differences in the DS, results from IHC analysis show the population density of PV+ cells (see **Table 5**), the density of VVA+ cells (see **Table 6**), the percentage of VVA+ cells with PV expression (see **Table 7**), and percentage of PV+ cells surrounded by VVA (see **Table 8**), present in the DMS and DLS of male and female, C57 and BTBR mice.

Table 5 / Mean and standard deviation (SD) of PV+ cell density (cells/mm²) in the Dorsomedial (DMS) and Dorsolateral Striatum (DLS) of male and female, C57 and BTBR mice.

		PV+ Cell Density (cells/mm ²)		
		DMS (SD)	DLS (SD)	Row Means (SD)
C57	Male	24.92 (3.89)	28.30 (3.67)	26.61 (3.99)
	Female	26.68 (2.04)	26.64 (3.83)	26.66 (2.89)
	Column Means	25.80 (3.07)	27.47 (3.64)	
BTBR	Male	14.66 (3.25)	30.46 (4.70)	22.56 (9.16)
	Female	13.68 (1.59)	24.20 (3.32)	18.94 (6.06)
	Column Means	14.17 (2.47)	27.33 (5.06)	

Table 6 / Mean and standard deviation (SD) of VVA+ cell density (cells/mm²) in the Dorsomedial (DMS) and Dorsolateral Striatum (DLS) of male and female, C57 and BTBR mice.

		VVA+ Cell Density (cells/mm ²)		
		DMS (SD)	DLS (SD)	Row Means (SD)
C57	Male	31.90 (5.45)	29.26 (3.40)	30.58 (4.51)
	Female	28.80 (2.68)	29.04 (4.58)	28.92 (3.54)
	Column Means	30.35 (4.37)	29.15 (3.80)	
BTBR	Male	28.32 (3.00)	26.54 (5.11)	27.43 (4.06)
	Female	27.40 (4.35)	29.54 (2.07)	28.47 (3.40)
	Column Means	27.86 (3.56)	28.04 (4.00)	

Table 7 | Mean and standard deviation (SD) Percentage of VVA+ cells with PV expression in the Dorsomedial (DMS) and Dorsolateral Striatum (DLS) of male and female, C57 and BTBR mice.

		% of VVA+ cells with PV expression		
		DMS (SD)	DLS (SD)	Row Means (SD)
C57	Male	49.60 (10.57)	80.02 (2.22)	64.81 (17.57)
	Female	67.56 (8.76)	82.80 (6.93)	75.18 (10.96)
	Column Means	58.58 (13.17)	81.41 (5.07)	
BTBR	Male	34.46 (6.08)	78.58 (6.10)	56.52 (23.95)
	Female	45.96 (4.57)	74.34 (5.58)	60.15 (15.71)
	Column Means	40.21 (7.90)	76.46 (5.95)	

Table 8 | Mean and standard deviation (SD) Percentage of PV+ cells surrounded by VVA in the Dorsomedial (DMS) and Dorsolateral Striatum (DLS) of male and female, C57 and BTBR mice.

		% of PV+ cells surrounded by VVA		
		DMS (SD)	DLS (SD)	Row Means (SD)
C57	Male	63.42 (12.85)	83.62 (2.28)	73.52 (13.75)
	Female	72.08 (4.46)	88.90 (3.38)	80.49 (9.62)
	Column Means	67.75 (10.15)	86.26 (3.89)	
BTBR	Male	70.62 (9.27)	68.46 (5.69)	69.54 (7.34)
	Female	90.24 (2.66)	90.88 (4.19)	90.56 (3.32)
	Column Means	80.43 (12.17)	79.67 (12.72)	

3.3 Subregional & Sex Differences in C57 mice

After looking at the overall DS for differences between the C57 and BTBR mice, we next focus on investigating for differences between the subregions (DMS and DLS) and also for any differences that may be due to sex of the C57 mice. A two-way ANOVA was performed to analyse the effects of region and sex on PV+ cell density in C57 mice (**Figure 7A**). Simple main effects analysis showed that region did not have a statistically significant effect on the density of PV+ cells ($F_{(1,16)} = 1.18, p = .294$). Simple main effects analysis also showed that sex did not have a significant effect on the density of PV+ cells ($F_{(1,16)} < 1, p = .975$). There was no statistically significant interaction between the effects of region and sex ($F_{(1,16)} = 1.23, p = .283$). Overall, these results suggest that there are no differences in PV+ IN densities between regions and sexes in C57 mice.

A two-way ANOVA was performed to analyse the effects of region and sex on VVA+ cell density in C57 mice (**Figure 7B**). Simple main effects analysis showed that region did not have a statistically significant effect on the density of VVA+ cells ($F_{(1,16)} = 0.41, p = .529$). Simple main effects analysis also showed that sex did not have a significant effect on the density of PV+ cells ($F_{(1,16)} = 0.79, p = .386$). There was no statistically significant interaction between the effects of region and sex ($F_{(1,16)} = 0.60, p = .451$). Overall, these results suggest that there are no differences in PNN densities between regions and sexes in C57 mice.

A two-way ANOVA was performed to analyse the effects of region and sex on the percentage of VVA+ cells with PV expression in C57 mice. Simple main effects analysis showed that sex did have a statistically significant effect on the percentage of VVA+ cells with PV expression ($F_{(1,16)} = 8.91, p = .009$). These results suggest that across both regions, the percentage of VVA+ cells with PV expression was significantly higher in female mice ($75.18 \pm 10.96\%$) compared to male mice ($64.81 \pm 17.57\%$). Simple main effects analysis showed that region also had a significant effect on the percentage of VVA+ cells with PV expression ($F_{(1,16)} = 43.18, p < .001$). These results suggest that across both sexes, the percentage of VVA+ cells with PV expression was significantly higher in the DLS ($81.41 \pm 5.67\%$) compared to the DMS ($58.58 \pm 13.17\%$). There was also a statistically significant interaction between the effects of region and sex ($F_{(1,16)} = 4.77, p = .044$).

Post hoc testing using Tukey's multiple comparisons test indicated that the percentage of VVA+ cells with PV expression in male C57 mice was significantly higher in the DLS ($80.02 \pm 2.22\%$) than in the DMS ($49.60 \pm 10.57\%$; $p < .001$, **Figure 7C**). Likewise, the percentage of VVA+ cells with PV expression in female C57 mice was significantly higher in the DLS ($82.80 \pm 6.93\%$) than in the DMS ($67.56 \pm 8.76\%$; $p = .031$, **Figure 7C**). These results suggest that in both sexes, C57 mice have a greater percentage of VVA+ cells with PV expression in the DLS than in the DMS. Additionally, female C57 mice ($67.56 \pm 8.76\%$) have a significantly higher percentage of VVA+ cells with PV expression in the DMS compared to C57 males ($49.60 \pm 10.57\%$; $p = .010$, **Figure 7C**), which suggest that C57 mice have a sex linked difference in the DMS in terms of PV expression.

A two-way ANOVA was performed to analyse the effects of region and sex on the percentage of PV+ cells surrounded by VVA in C57 mice. Simple main effects analysis showed that sex did have a statistically significant effect on the percentage of PV+ cells surrounded by VVA ($F_{(1,16)} = 4.82, p = .043$). These results suggest that across both regions, the percentage

of PV+ cells surrounded by VVA was significantly higher in female mice ($80.49 \pm 9.62\%$) compared to male mice ($73.52 \pm 13.75\%$). Simple main effects analysis showed that region also had a significant effect on the percentage of PV+ cells surrounded by VVA ($F_{(1,16)} = 34.00$, $p < .001$). These results suggest that across both sexes, the percentage of PV+ cells surrounded by VVA was significantly higher in the DLS ($86.26 \pm 3.89\%$) compared to the DMS ($67.75 \pm 10.15\%$). There was no statistically significant interaction between the effects of region and sex ($F_{(1,16)} < 1$, $p = .602$).

Post hoc testing using Tukey's multiple comparisons test indicated that the percentage of PV+ cells surrounded by VVA in male C57 mice was significantly higher in the DLS ($83.62 \pm 2.28\%$) than in the DMS ($63.42 \pm 12.85\%$; $p = .002$, **Figure 7D**). Likewise, the percentage of PV+ cells surrounded by VVA in female C57 mice was significantly higher in the DLS ($88.90 \pm 3.38\%$) than in the DMS ($72.08 \pm 4.46\%$; $p = .009$, **Figure 7D**). These results suggest that regardless of sex, PV+ INs in the DLS of C57 mice are more colocalised with PNNs than in the DMS, male mice having ~20% more PV+ INs colocalised with PNNs and female mice with ~17% more PV+ INs colocalised with PNNs in the DLS.

In conclusion, C57 mice were found to not possess any significant differences between region and sex in terms of PV+ and VVA+ cells densities. However, in terms of VVA+ cells with PV expression, we observe lower percentages in the DMS compared to the DLS. Finally, the results show that the percentage of PV+ cells surrounded by VVA was higher in the DLS than in the DMS for both sexes in C57 mice.

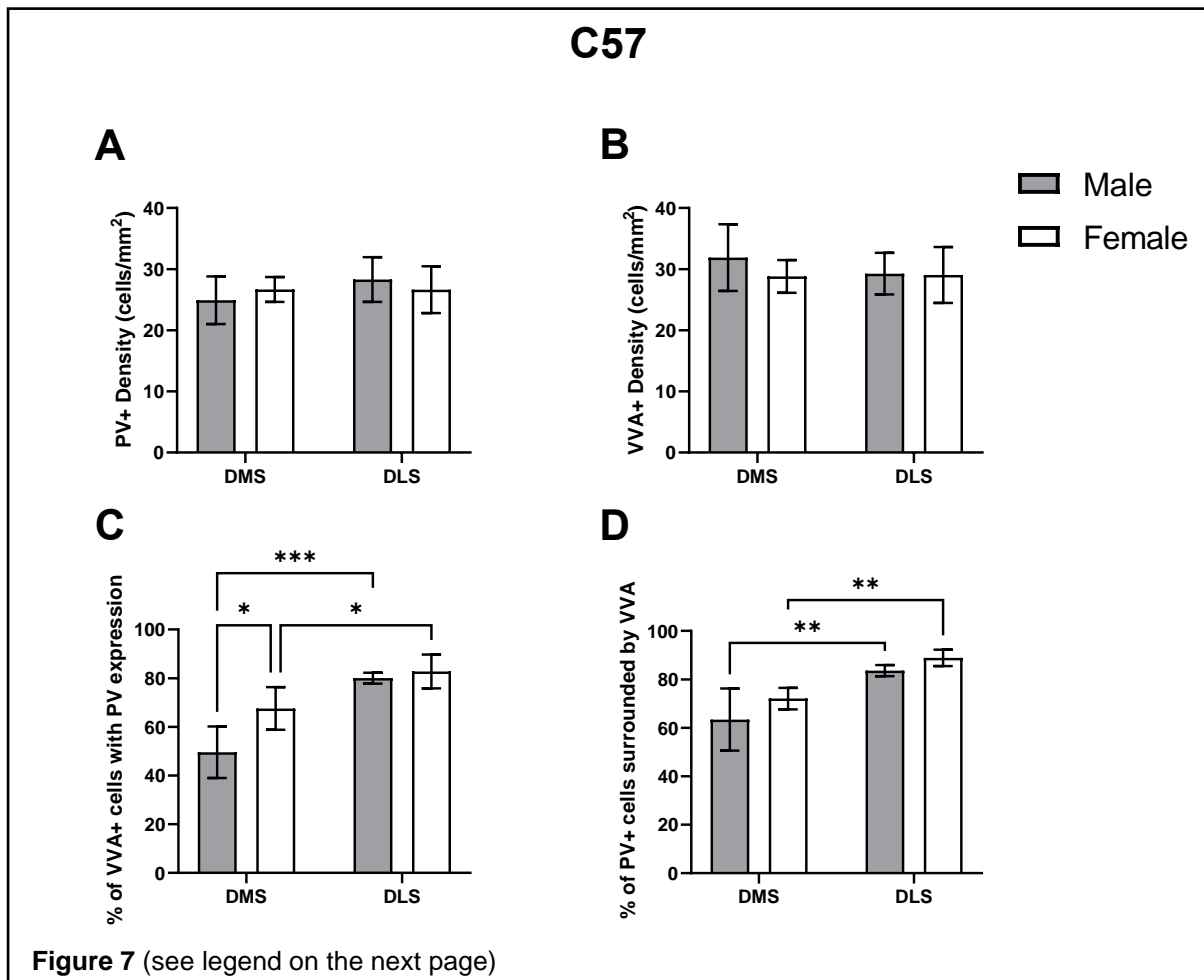


Figure 7 | Bar charts showing mean (\pm SD) PV+ cell density (**A**), mean (\pm SD) VVA+ cell density (**B**), mean (\pm SD) percentage of VVA+ cells with PV expression (**C**), and mean (\pm SD) percentage of PV+ cells surrounded by VVA (**D**) in the Dorsomedial (DMS) and Dorsolateral Striatum (DLS) of male and female C57 mice. Asterisks represent * $p \leq 0.05$, ** $p \leq 0.01$, and *** $p \leq 0.001$, respectively

3.4 Subregional & Sex Differences in BTBR mice

Similarly, to the analysis carried out on the C57 mice, BTBR mice were also investigated for subregional differences (DMS and DLS) and for any sex differences. A two-way ANOVA was performed to analyse the effects of region and sex on PV+ cell density in BTBR mice. Simple main effects analysis showed that region did have a statistically significant effect on the density of PV+ cells ($F_{(1,16)} = 74.87$, $p < .001$). These results suggest that across both sexes, PV+ cell density was significantly higher in the DLS (27.33 ± 5.06 cells/mm²) than in the DMS (14.17 ± 2.47 cells/mm²). Simple main effects analysis also showed that sex did have a significant effect on the density of PV+ cells ($F_{(1,16)} = 5.67$, $p = .030$). These results suggest that across both regions, PV+ cell density was significantly lower in female mice

(18.94 ± 6.06 cells/mm²) than in male mice (22.56 ± 9.16 cells/mm²). There was no statistically significant interaction between the effects of region and sex ($F_{(1,16)} = 3.01, p = .102$).

Post hoc testing using Tukey's multiple comparisons test revealed that PV+ cell density in male BTBR mice was significantly lower in the DMS (14.66 ± 3.25 cells/mm²) than in the DLS (30.46 ± 4.70 cells/mm²; $p < .001$, **Figure 8A**). Similarly, PV+ cell density in female BTBR mice was significantly lower in the DMS (13.68 ± 1.59 cells/mm²) than in the DLS (24.20 ± 3.32 cells/mm²; $p < .001$, **Figure 8A**). These results suggest that regardless of sex, density of PV+ INs in the DMS of BTBR mice are lower than in the DMS, male mice possessing ~52% less PV+ INs and female mice with ~43% less PV+ INs in the DMS compared to the DLS. A Tukey's multiple comparisons test additionally revealed that the density of PV+ cells in the DLS region was significantly lower in female BTBR mice (24.20 ± 3.32 cells/mm²) than in male BTBR mice (30.46 ± 4.70 cells/mm²; $p = .045$, **Figure 8A**). These results in turn suggest of a sex difference within the DLS region in BTBR mice.

A two-way ANOVA was performed to analyse the effects of region and sex on VVA+ cell density in BTBR mice (**Figure 8B**). Simple main effects analysis showed that region did not have a statistically significant effect on the density of VVA+ cells ($F_{(1,16)} < 1, p = .917$). Simple main effects analysis also showed that sex did not have a significant effect on the density of VVA+ cells ($F_{(1,16)} < 1, p = .551$). There was no statistically significant interaction between the effects of region and sex ($F_{(1,16)} = 1.32, p = .268$). As expected, these results indicate that PNN density is not affected by region or sex in BTBR mice.

A two-way ANOVA was performed to analyse the effects of region and sex on the percentage of VVA+ cells with PV expression in BTBR mice. Simple main effects analysis showed that region did have a significant effect on the percentage of VVA+ cells with PV expression ($F_{(1,16)} = 208.4, p < .001$). These results suggest that regardless of sex, percentage of VVA+ cells with PV expression in BTBR mice was ~36% lower in the DMS than in the DLS, also confirming that BTBR have a regional difference in the DS. Simple main effects analysis showed that sex did not have a statistically significant effect on percentage of VVA+ cells with PV expression ($F_{(1,16)} = 2.09, p = .168$). There was also a statistically significant interaction between the effects of region and sex ($F_{(1,16)} = 9.82, p = .006$).

Post hoc testing using Tukey's multiple comparisons test indicated that the percentage of VVA+ cells with PV expression in male BTBR mice was significantly higher in the DLS ($78.58 \pm 6.10\%$) than in the DMS ($34.46 \pm 6.08\%$; $p < .001$, **Figure 8C**). Likewise, the

percentage of VVA+ cells with PV expression in female BTBR mice was significantly higher in the DLS ($74.34 \pm 5.58\%$) than in the DMS ($45.96 \pm 4.57\%$; $p < .001$, **Figure 8C**). These results suggest that in both sexes, BTBR mice have a greater percentage of VVA+ cells with PV expression in the DLS than in the DMS. Additionally, female BTBR mice ($45.96 \pm 4.57\%$) have a significantly higher percentage of VVA+ cells with PV expression in the DMS compared to C57 males ($34.46 \pm 6.08\%$; $p = .024$, **Figure 8C**).

A two-way ANOVA was performed to analyse the effects of region and sex on the percentage of PV+ cells surrounded by VVA in BTBR mice. Simple main effects analysis showed that region did not have a statistically significant effect on percentage of PV+ cells surrounded by VVA ($F_{(1,16)} < 1$, $p = .984$). Simple main effects analysis showed that sex did have a significant effect on the percentage of PV+ cells surrounded by VVA ($F_{(1,16)} = 47.99$, $p < .001$). There was no statistically significant interaction between the effects of region and sex ($F_{(1,16)} < 1$, $p = .920$).

Post hoc testing using Tukey's multiple comparisons test revealed that percentage of PV+ cells surrounded by VVA in BTBR mice was significantly higher in the DMS region of female mice ($90.24 \pm 2.66\%$) than in male mice ($70.62 \pm 9.27\%$; $p < .001$, **Figure 8D**). Similarly, this was also observed in the DLS region where the percentage of PV+ cells surrounded by VVA was significantly higher in female mice ($90.88 \pm 4.19\%$) than in male mice ($70.62 \pm 5.69\%$; $p < .001$, **Figure 8D**). These results show that female BTBR mice possess a greater percentage of PV+ INs ensheathed by PNNs in both the DMS and DLS regions compared to male counterparts, indicating a sex difference in BTBR mice.

In contrast to the C57 mice, BTBR mice were found to have a significantly reduced density of PV+ INs in the DMS compared to the DLS. However, like in the C57 mice, the density of PNNs was unaltered, suggesting PV is downregulated in the DMS but not on the DLS. Lower percentage of VVA+ cells with PV expression in the DMS but not in the DLS further support this. Here we also observe that BTBR mice do not show a higher percentage of PV+ cells surrounded by VVA in the DLS than in the DMS like the C57 mice. Rather we observe a sex difference in BTBR mice, with female mice showing a higher percentage of PV+ cells surrounded by VVA, which was not found in the C57 mice.

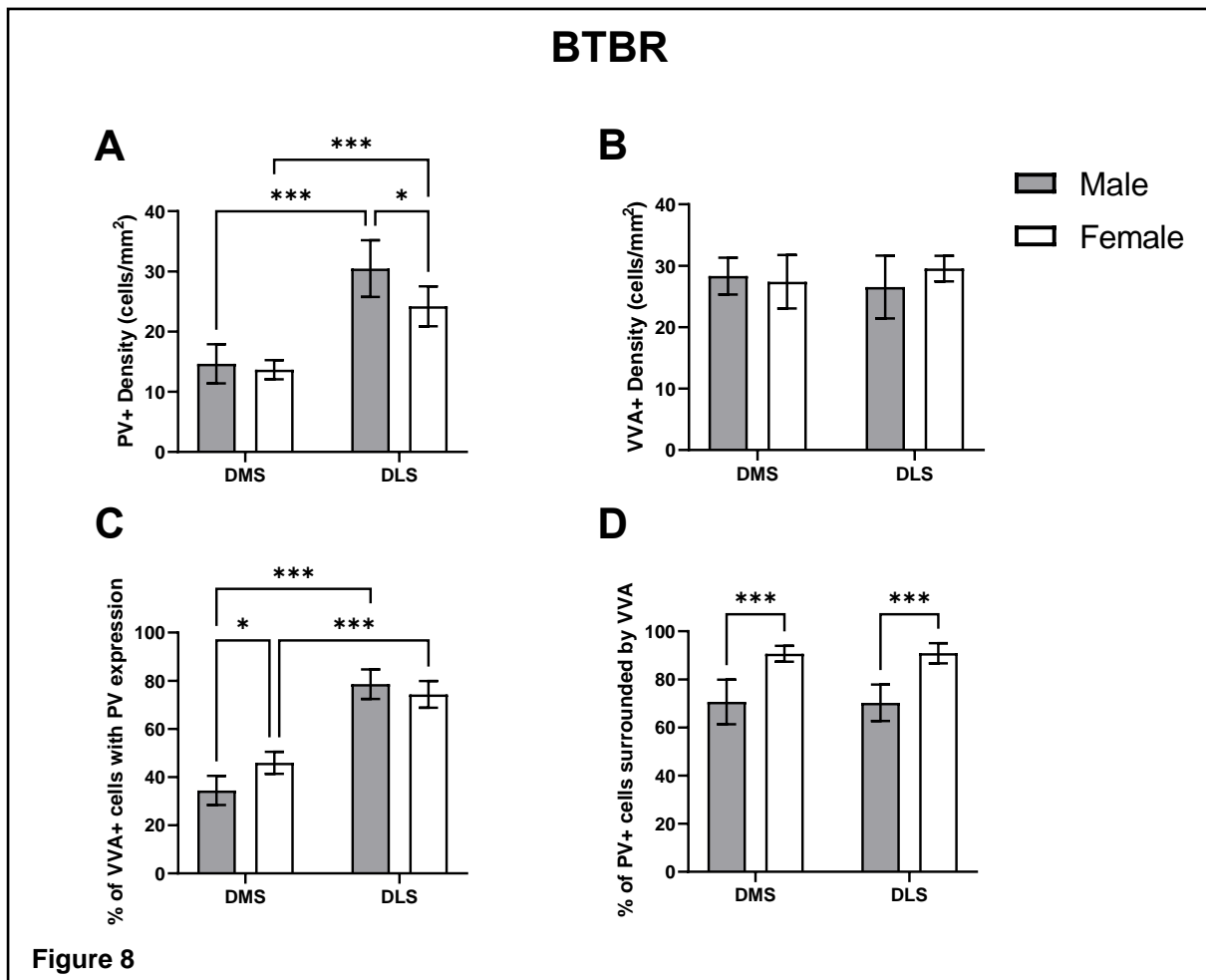


Figure 8 | Bar charts showing mean (\pm SD) PV+ cell density (A), mean (\pm SD) VVA+ cell density (B), mean (\pm SD) percentage of VVA+ cells with PV expression (C), and mean (\pm SD) percentage of PV+ cells surrounded by VVA (D) in the Dorsomedial (DMS) and Dorsolateral Striatum (DLS) of male and female C57 mice. Asterisks represent * $p \leq 0.05$, and *** $p \leq 0.001$, respectively.

3.5 Dorsomedial Striatum

Finally, this study investigated the individual regions, starting with the DMS, to compare the BTBR mice to the C57 for differences between the animal model. A two-way ANOVA was performed to analyse the effects of animal model and sex on PV+ cell density in the DMS. Simple main effects analysis showed that sex did not have a statistically significant effect on the density of PV+ cells ($F_{(1,16)} < 1$, $p = .763$). Simple main effects analysis found that the animal model did have a significant effect on the density of PV+ cells ($F_{(1,16)} = 83.42$, $p < .001$). These results suggest that across both sexes, density of PV+ cells was significantly lower in BTBR mice (14.17 ± 2.47 cells/mm²) than in C57 mice (25.80 ± 3.07 cells/mm²). There was no statistically significant interaction between the effects of animal model and sex ($F_{(1,16)} = 1.16$, $p = .298$).

Post hoc testing using Tukey's multiple comparisons test revealed the density of PV+ cells in the DMS of male mice was significantly lower in BTBR mice (14.66 ± 3.25 cells/mm²) than in C57 mice (24.92 ± 3.89 cells/mm²; $p < .001$, **Figure 9A**). Likewise, the density of PV+ cells in the DMS of female mice was significantly lower in BTBR mice (13.68 ± 1.59 cells/mm²) than in C57 mice (26.68 ± 2.04 cells/mm²; $p < .001$, **Figure 9A**). These results suggest that regardless of sex, density of PV+ INs in the DMS of BTBR mice are lower than in the DMS of C57 mice. Compared to control counterparts, male and female BTBR show to have a ~41% and ~49% decrease in PV+ IN density, respectively (see **Figure 9E**).

A two-way ANOVA was performed to analyse the effects of animal model and sex on VVA+ cell density in the DMS. Simple main effects analysis showed that sex did not have a statistically significant effect on the density of VVA+ cells ($F_{(1,16)} = 1.25$, $p = .281$). Simple main effects analysis found that animal model also did not have a significant effect on the density of VVA+ cells ($F_{(1,16)} = 1.91$, $p = .186$). There was no statistically significant interaction between the effects of model and sex ($F_{(1,16)} < 1$, $p = .553$). These results suggest PNN densities are unaltered in the DMS region between the C57 and BTBR mice models. Combined with the significant results of reduced PV+ IN density in BTBR mice, these results suggest that Pvalb neurons are not lost (due to unaltered densities of PNNs, see **Figure 9B & 9E**).

A two-way ANOVA was performed to analyse the effects of animal model and sex on the percentage of VVA+ cells with PV expression in the DMS. Simple main effects analysis showed that model had a significant effect on the percentage of VVA+ cells with PV expression

($F_{(1,16)} = 27.42, p < .001$). These results suggest that across both sexes, the percentage of VVA+ cells with PV expression was significantly lower in BTBR mice ($40.21 \pm 7.90\%$) than in C57 mice ($58.58 \pm 13.17\%$). Simple main effects analysis showed that sex also had a significant effect on the percentage of VVA+ cells with PV expression ($F_{(1,16)} = 17.63, p < .001$). These results suggest that across both animal models, the percentage of VVA+ cells with PV expression was significantly lower in male mice ($42.03 \pm 11.39\%$) than in female mice ($56.76 \pm 13.15\%$). There was no statistically significant interaction between the effects of model and sex ($F_{(1,16)} < 1, p = .371$).

Post hoc testing using Tukey's multiple comparisons test revealed that the percentage of VVA+ cells with PV expression in the DMS of male mice was significantly lower in BTBR mice ($34.46 \pm 6.08\%$) than in C57 mice ($49.60 \pm 10.57\%$; $p = .035$, **Figure 9C**.) Likewise, the percentage of VVA+ cells with PV expression in the DMS of female mice was significantly lower in BTBR mice ($45.96 \pm 4.57\%$) than in C57 mice ($67.56 \pm 8.76\%$; $p = .002$, **Figure 9C**). Indicating that PV expression is reduced in the DMS of BTBR mice. Tukey's multiple comparisons test also revealed that the percentage of VVA+ cells with PV expression in the DMS of C57 mice was significantly lower in male mice ($49.60 \pm 10.57\%$) than in female mice ($67.56 \pm 8.76\%$; $p = .011$, **Figure 9C**), suggesting that male C57 mice have a lower PV expression than female mice.

A two-way ANOVA was performed to analyse the effects of animal model and sex on the percentage of PV+ cells surrounded by VVA in the DMS. Simple main effects analysis showed that animal model did have a statistically significant effect on the percentage of PV+ cells surrounded by VVA ($F_{(1,16)} = 11.58, p = .004$). These results suggest that across both sexes, the percentage of PV+ cells surrounded by VVA was significantly higher in BTBR mice ($80.43 \pm 12.17\%$) than in C57 mice ($67.75 \pm 10.15\%$). Simple main effects analysis showed that sex also had a significant effect on the percentage of PV+ cells surrounded by VVA ($F_{(1,16)} = 14.40, p = .002$). These results suggest that across both animal models, the percentage of PV+ cells surrounded by VVA was significantly lower in male mice ($67.75 \pm 11.22\%$) than in female mice ($80.43 \pm 10.18\%$). There was no statistically significant interaction between the effects of model and sex ($F_{(1,16)} = 2.16, p = .161$).

Post hoc testing using Tukey's multiple comparisons test revealed that the percentage of PV+ cells surrounded by VVA in the DMS of female mice was significantly higher in BTBR mice ($90.24 \pm 2.66\%$) than in C57 mice ($72.08 \pm 4.46\%$; $p = .016$, **Figure 9D**). These results

suggest that female BTBR possess ~18% more PV+ INs which are enwrapped by PNNs in the DMS than control female mice. There was however no significant difference in the percentage of PV+ cells surrounded by VVA in the DMS between the male BTBR and male C57 mice ($p = .537$, **Figure 9D**). The multiple comparisons also found that the percentage of PV+ cells surrounded by VVA in the DMS of BTBR mice was significantly higher in females ($70.62 \pm 9.27\%$) than in males ($90.24 \pm 2.66\%$; $p = .009$, **Figure 9D**).

In conclusion, we observe that compared to C57 mice, BTBR show a significantly reduced density of PV+ INs in the DMS. This reduction is not followed by any significant differences in the density of PNNs and the percentage of VVA+ cells with PV expression is reduced in BTBR mice, indicating that BTBR are showing reduced PV expression, not a loss of Pvalb INs, in the DMS. Again, we also observe that the percentage of PV+ cells surrounded by VVA is higher in female BTBR mice than male mice suggesting a sex difference, but we also observe the colocalisation percentage to be higher for female BTBR than female C57 mice.

Dorsomedial Striatum

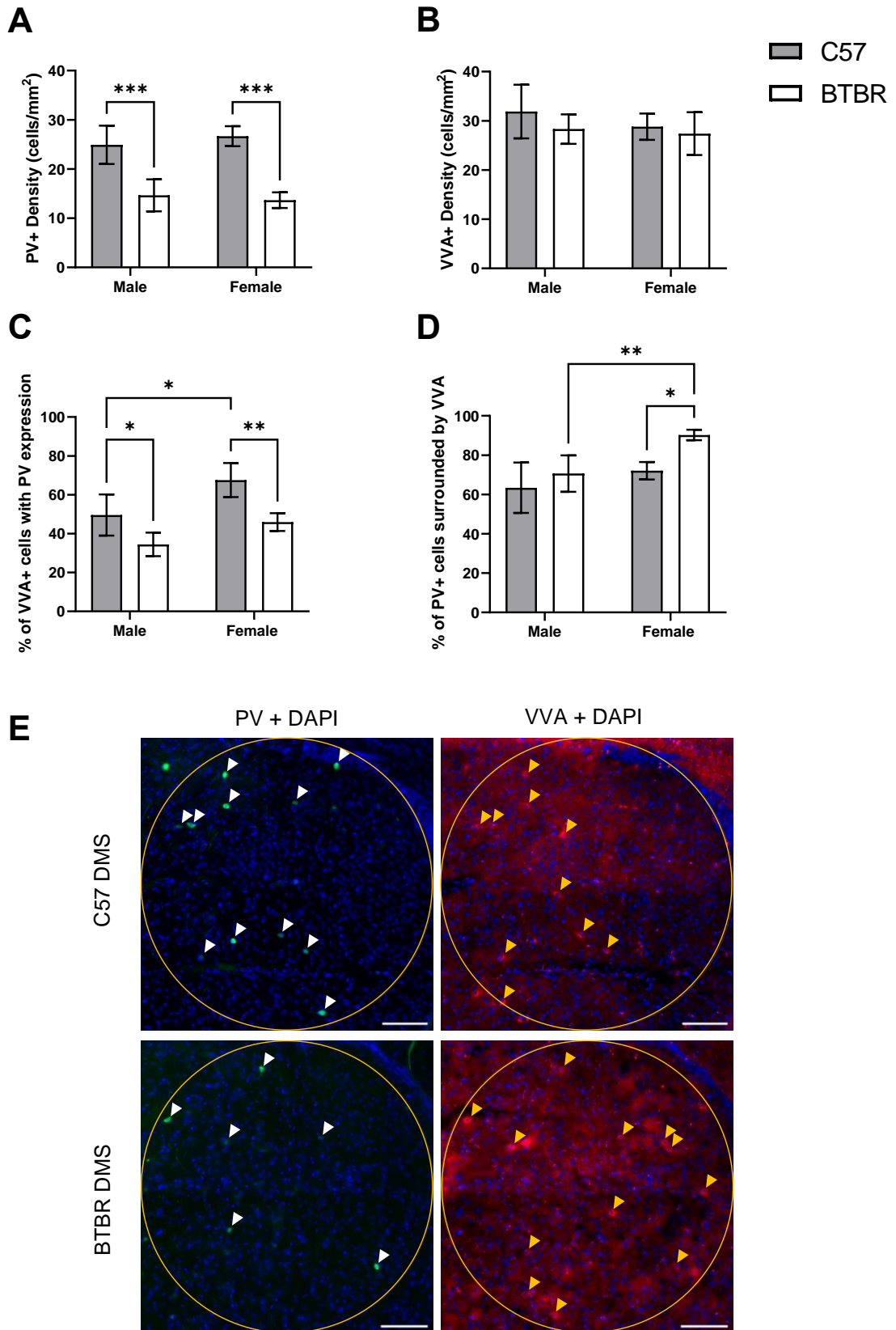


Figure 9 (see legend on the next page)

Figure 9 | Bar chart showing mean (\pm SD) PV+ cell density (A), mean (\pm SD) VVA+ cell density (B), and mean (\pm SD) percentage of VVA+ cells with PV expression (C), and mean (\pm SD) percentage of PV+ cells surrounded by VVA (C) in the Dorsomedial Striatum (DMS) of male and female C57 (grey) and BTBR (white) mice. Asterisks represent * $p \leq 0.05$, ** $p \leq 0.01$, and *** $p \leq 0.001$, respectively (D) Representative immunofluorescence images of PV+ cells (white triangles) and VVA+ cells (yellow triangles) from the DMS of a C57 and BTBR mice with an approx. similar ROI area (mm^2), counterstained with DAPI. Scale bar: $100\mu\text{m}$

3.6 Dorsolateral Striatum

For a complete analysis, the DLS was investigated similarly to that of the DMS. A two-way ANOVA was performed to analyse the effects of animal model and sex on PV+ cell density in the DLS. Simple main effects analysis found that model did not have a significant effect on the density of PV+ cells ($F_{(1,16)} < 1$, $p = .937$). These results suggest that the density of PV+ INs is unaffected in the DLS of BTBR mice (**Figure 10A**). Simple main effects analysis showed that sex did have a statistically significant effect on the density of PV+ cells ($F_{(1,16)} = 5.12$, $p = .038$). These results suggest that across both animal models, the density of PV+ cells was significantly higher in male mice (29.38 ± 7.18 cells/ mm^2) compared to female mice (25.42 ± 8.70 cells/ mm^2). There was no statistically significant interaction between the effects of model and sex ($F_{(1,16)} = 1.73$, $p = .207$).

A two-way ANOVA was performed to analyse the effects of animal model and sex on VVA+ cell density in the DLS. Simple main effects analysis found that model did not have a significant effect on the density of VVA+ cells ($F_{(1,16)} < 1$, $p = .540$). Simple main effects analysis showed that sex did not have a statistically significant effect on the density of VVA+ cells ($F_{(1,16)} < 1$, $p = .445$). These results show that in the DLS there is no significant difference in PNN density between animal models as well as between sexes (**Figure 10B**). The two-way ANOVA revealed that there was no statistically significant interaction between the effects of model and sex ($F_{(1,16)} < 1$, $p = .378$).

A two-way ANOVA was performed to analyse the effects of animal model and sex on the percentage of VVA+ cells with PV expression in the DMS. Simple main effects analysis showed that model did not have a significant effect on the percentage of VVA+ cells with PV expression ($F_{(1,16)} = 4.15$, $p = .059$). These results suggest that across both sexes, the percentage of VVA+ cells with PV expression was not significantly different between C57 and BTBR mice (**Figure 10C**). Simple main effects analysis showed that sex also did not have a significant effect on the percentage of VVA+ cells with PV expression ($F_{(1,16)} < 1$, $p = .742$). These results suggest that across both animal models, the percentage of VVA+ cells with PV expression was

not significantly different between male and female mice (**Figure 10C**). There was no statistically significant interaction between the effects of model and sex ($F_{(1,16)} = 1.89, p = .188$).

A two-way ANOVA was performed to analyse the effects of animal model and sex on the percentage of PV+ cells surrounded by VVA in the DLS. Simple main effects analysis showed that model had a significant effect on the percentage of PV+ cells surrounded by VVA ($F_{(1,16)} = 13.04, p = .002$). These results suggest that across both sexes the percentage of PV+ cells surrounded by VVA in the DLS was significantly higher in C57 mice ($86.26 \pm 3.89\%$) than in BTBR mice ($79.67 \pm 12.72\%$). Simple main effects analysis showed that sex also had a statistically significant effect on the percentage of PV+ cells surrounded by VVA ($F_{(1,16)} = 57.61, p < .001$). These results suggest that across both animal models, the percentage of PV+ cells surrounded by VVA in the DLS was significantly higher in female mice ($89.89 \pm 3.74\%$) than in male mice ($76.04 \pm 8.97\%$). The two-way ANOVA also revealed a statistically significant interaction between the effects of model and sex ($F_{(1,16)} = 22.06, p < .001$).

Post hoc testing using Tukey's multiple comparisons test indicated that in the DLS of male mice was significantly lower in BTBR mice ($68.46 \pm 5.69\%$) than in male C57 mice ($83.62 \pm 2.28\%$; $p < .001$, **Figure 10D & E**). The multiple comparisons test also indicated that the percentage of PV+ cells surrounded by VVA in BTBR mice was lower in males ($68.46 \pm 5.69\%$) than in females ($90.88 \pm 4.19\%$; $p < .001$, **Figure 10D**). There was no significant difference in the percentage of PV+ cells surrounded by VVA in the DLS between female BTBR and female C57 mice ($p = .868$, **Figure 10D**). These results suggest that male, but not female, BTBR mice have ~15% less PV+ INs which are enwrapped by PNNs in the DLS than control mice.

Unlike in the DMS, we do not observe BTBR to have a reduced expression of PV in the DLS. However, we do observe that male BTBR mice have a significantly lower percentage of PV+ cells surrounded by VVA compared to C57 males. Our results also indicate that there may be a sex difference in the BTBR mice with males having a lower percentage of PV+ cells surrounded by VVA than females.

Dorsolateral Striatum

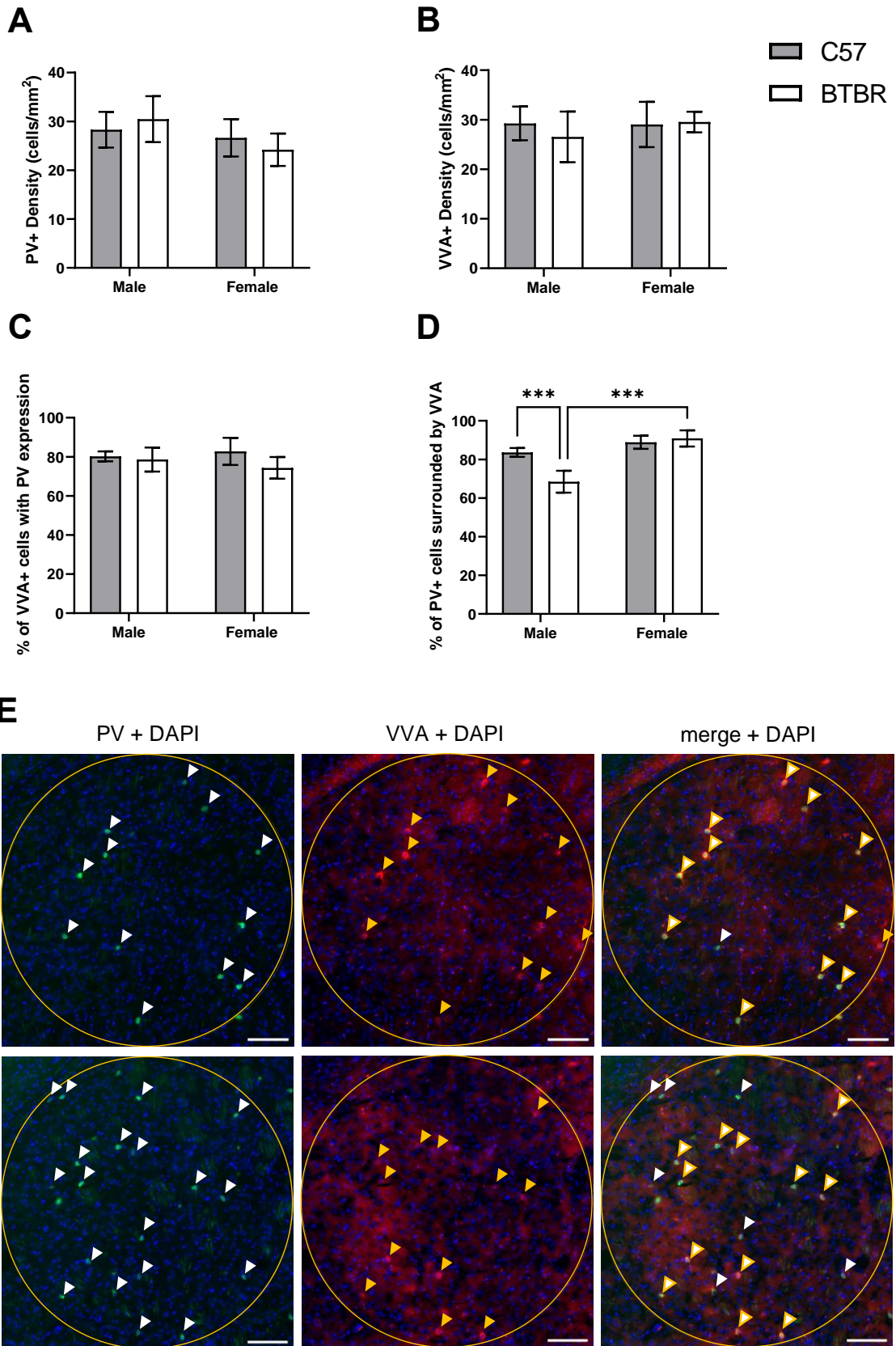


Figure 10 (see legend on the next page)

Figure 10 | Bar chart showing mean (\pm SD) PV+ cell density (A), mean (\pm SD) VVA+ cell density (B), and mean (\pm SD) percentage colocalisation of PV+VVA+ cells (C) in the Dorsolateral Striatum (DLS) of male and female C57 (grey) and BTBR (white) mice. Asterisks represent *** $p \leq 0.001$. (D) Representative immunofluorescence images of PV+ cells (white triangles), VVA+ cells (yellow triangles), and PV+VVA+ cells (white triangle with yellow border) from the DLS of a male C57 and male BTBR mice, counterstained with DAPI. Scale bar: 100 μ m.

3.7 Western Blotting - PV Expression in the Striatum of BTBR mice

An unpaired, one-way t-test was conducted to compare the % of PV levels in the striatum of (male) BTBR mice (n = 5) to that of C57 mice (n = 5). Expression of PV for C57 and BTBR mice was quantified using Western Blotting and β -actin was used as a loading control for the normalisation of the PV signal (Figure 11A; see Appendix D to compare location of bands along molecular weight (kDa) ladder). PV expression was defined as 100%. There was a significant difference in the % of PV levels in C57 mice (100%, SEM \pm 13.43) and BTBR mice (69.87%, SEM \pm 8.38; $t(8) = 1.90$, $p = .047$, Figure 11B). These results suggest that in the striatum, BTBR mice present with a ~30% reduction in PV expression compared to control mice.

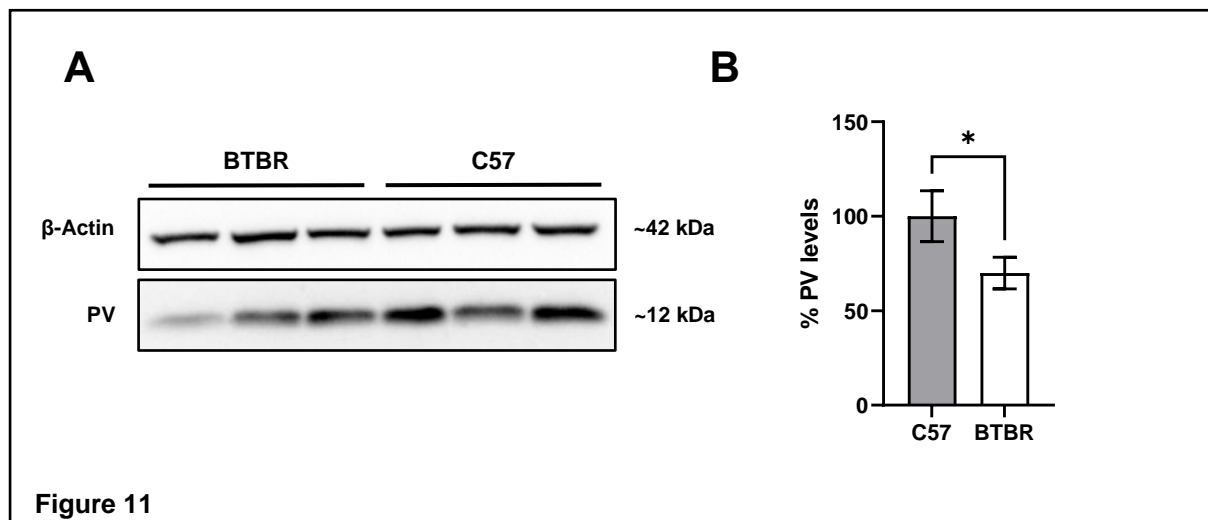


Figure 11 | (A) Representative Western Blot and (B) quantification of PV levels in the male C57 and BTBR mice. β -actin was used as a loading control for the normalisation of the PV signal. Results are expressed as a percentage of normalised PV levels measured in control (C57), defined as 100%. Asterisks represent * $p \leq 0.05$. Data was collated from three independent experiments (two membranes per experiment) and shown as mean \pm SEM.

3.8 Summary Table of Results

Table 9 | Summary table of results, linking to the hypotheses in this study and the relevant figure.

	Mean (\pm SD)	p-value	Relevant Figure	Hypothesis
DS - PV+ cells per mm²				
C57	26.67 \pm 2.80	< .001	6A	1
BTBR	20.78 \pm 3.43			
DS - VVA+ cells per mm²				
C57	29.78 \pm 3.32	.260	6B	2
BTBR	27.97 \pm 3.38			
DS - Percentage of VVA+ cells with PV expression				
C57	70.04 \pm 7.71	< .001	6C	3
BTBR	58.36 \pm 4.72			
DS - Percentage of PV+ cells surrounded by VVA				
C57	77.03 \pm 5.86	.185	6D	4
BTBR	80.07 \pm 12.02			
C57 mice - PV+ cells per mm²				
DMS	25.80 \pm 3.07	.294	7A	5
DLS	27.47 \pm 3.64			
C57 mice - VVA+ cells per mm²				
DMS	30.55 \pm 4.37	.529	7B	6
DLS	29.15 \pm 3.80			
C57 mice - Percentage of VVA+ cells with PV expression				
DMS	58.58 \pm 13.17	.044	7C	7
DLS	81.41 \pm 5.07			
C57 mice - Percentage of PV+ cells surrounded by VVA				
DMS	67.75 \pm 10.15	< .001	7D	8
DLS	86.26 \pm 3.89			
DMS - PV+ cells per mm²				
C57	25.80 \pm 3.07	< .001	9A & 9E	9
BTBR	14.17 \pm 2.47			
DMS - VVA+ cells per mm²				
C57	30.35 \pm 4.37	.186	9B & 9E	10
BTBR	27.86 \pm 3.57			

DMS - Percentage of VVA+ cells with PV expression				
C57	58.58 ± 13.17	< .001	9C	11
BTBR	40.21 ± 7.90			
DMS - Percentage of PV+ cells surrounded by VVA				
C57	67.75 ± 10.15	.004	9D	12
BTBR	80.43 ± 12.17			
DLS - PV+ cells per mm² in BTBR mice				
Male	30.46 ± 4.70	.045	8A	13
Female	24.20 ± 3.32			
DMS - Percentage of PV+ cells surrounded by VVA in BTBR mice				
Male	70.62 ± 9.27	.001	8D	14
Female	90.24 ± 2.66			
DLS - Percentage of PV+ cells surrounded by VVA in BTBR mice				
Male	68.46 ± 5.69	.001	8D	1
Female	90.88 ± 4.19			
	Mean (±SEM)	p-value	Relevant Figure	Hypothesis
Striatum – PV Expression (%)				
C57	100 ± 13.43	.047	11A & 11B	16
BTBR	69.87 ± 8.38			

4.0 DISCUSSION

The most recent research demonstrates that transgenic and one environmental ASD mice models present with a reduction in the PV protein expression, rather than the previously deduced loss of the Pvalb neurons themselves (Filice et al., 2016; Lauber et al., 2016; 2018). This common endpoint observed in such mice has fundamentally led to the creation of ‘The Parvalbumin Hypothesis of Autism Spectrum Disorder’, also supported by various other research, which indicates that the endpoint aetiology of ASD may be signified by a downregulated expression of PV (Filice et al., 2020). Yet, PV downregulation has not been investigated in an idiopathic model of ASD, such as the validated BTBR T⁺ Itpr3^{tf}/J mouse model, which displays robust and consistent behavioural alterations with relevance to all human ASD core symptoms (McFarlane et al., 2008, Amodeo et al., 2019).

4.1 Decreased PV expression, but unaltered density of Pvalb interneurons in the dorsal striatum of BTBR mice

IHC analysis examined the dorsal striatum as a whole first. Collectively, BTBR mice showed a significant ~22% reduction in the density of PV+ INs, without a change in PNN density as indicated by the VVA+ cell staining. When accounted for sex, only female BTBR mice showed a decrease in PV+ INs density which was significant. For male BTBR mice, this reduction was not significant at the analysis level of DS. However, BTBR mice were found to have ~12% less VVA+ cells with PV expression in the DS compared to control mice, suggesting that in fact these mice are showing a reduced expression of PV. PV protein levels in the striatum was also observed to be reduced by ~30% as determined by WB analysis. Taken together these results show that idiopathic, BTBR mice have a decreased expression of PV, but not a loss of Pvalb INs, in the DS. Previous ASD models that underwent staining to visualise PNNs also showed fewer PV+ INs and an unchanged number of PNNs. A reduced number of PV+ INs were observed in the striatum of Shank 3B^{-/-} (-30%), Cntnap2^{-/-} (-30%), and in utero valproic acid (VPA)-treated mice (-15%; Filice et al., 2016; Lauber et al., 2016; 2018), which is similar to the reduction of PV+ INs this current study found in the dorsal striatum of BTBR mice (-22%). Moreover, in ASD mice models with such reductions in PV+ INs, decreased PV protein expression levels in the striatum were observed in Shank 3B^{-/-} (-50%), Cntnap2^{-/-} (-22%), and in utero VPA-treated mice (-30%; Filice et al., 2016; Lauber et al., 2016; 2018). These findings are also similar to this current study which observed a ~30% decrease in PV levels in the striatum of BTBR mice. Therefore, the results of this study are similar but

moreover consistent across both IHC and WB analysis with that of previous literature. These results once again indicate that striatal regions are a common hotspot for ASD-associated downregulation of PV across genetically modified, environmentally insulted, and now idiopathic mice models of ASD. These results are in line with the Parvalbumin Hypothesis, which suggests that decreased levels of PV are related to the aetiology of ASD (Filice et al., 2020). Establishing whether ASD mice models present with a loss of Pvalb INs, or a reduced expression of PV is of high importance since it is expected that such observations will alter the functioning of the neuronal network, hence the balance of E/I, in distinct ways. Functionally, a loss of these inhibitory, Pvalb neurons would be expected to result in a reduced inhibitory tone. Whereas a decrease in PV expression would mean that the decay of intracellular Ca^{2+} concentration ($[\text{Ca}^{2+}]_i$), evoked by action potentials, would be slower, promoting these inhibitory INs to further release GABA during the stimulation period, resulting in enhanced paired-pulse facilitation of inhibitory postsynaptic currents (IPSCs), and therefore, in theory, enhance their ability to exert inhibition onto striatal MSNs (Caillard et al., 2000; Müller et al., 2007; Orduz et al., 2013, Wöhr et al., 2015).

4.2 Dorsomedial striatum accounts for reduction in PV expression in BTBR mice

Compared to control mice, BTBR mice both male and female had a significantly reduced density of PV+ INs in the DMS, by ~41% and ~49% respectively. BTBR mice did not show such reduction in the DLS region. The findings were observed whilst densities of PNNs were not significantly different between the two models. Additionally, the results show that BTBR mice have ~22% (females) and ~15% (males) less VVA+ cells with PV expression in the DMS compared to the control mice. Combined, it can be concluded that BTBR mice exhibit a reduced expression of PV which is accounted by the DMS, and not the DLS region. This has been previously reported in the literature (Briones et al., 2021), making this a consistent finding which shows that the aetiology of ASD in BTBR mice is marked by PV downregulation in the DMS, and not the DLS. As a result, we would expect that electrophysiological properties of Pvalb INs in the DMS is altered. Previous work has demonstrated that striatal Pvalb INs with abolished expression of PV (PV^{-/-}) resulted in a significant increase of the second and third IPSC amplitude in MSNs, compared to WT MSNs, augmenting increased inhibition via paired pulse facilitation in such INs (Orduz et al., 2013). Increased mean amplitudes of mIPSC events relative to control mice have also been observed in the DMS of BTBR mice, indicating a particularly strong inhibitory response from PV+ INs to MSNs (Briones et al., 2021). The fact

that BTBR mice show this to be the case in the DMS fit with the findings of this study because this is the region which shows a downregulation of PV, and which previous research has shown this would result in increased inhibition. PV downregulation was not observed in the DLS therefore we would expect that this region does not have identical aetiology, highlighting the importance of investigating the medial and lateral regions of the DS as individual regions.

Alterations in the DMS have been previously implicated to affect the phenotype related to RRBI. The DMS has been shown to govern goal-directed behaviour and in particular it may be a key region involved in the circuitry of behavioural flexibility (Ragozzino et al., 2002). Microinfusion of a Serotonin 2A (5HT2A) receptor antagonist into the DMS has been shown to alleviate a reversal learning impairment and attenuate grooming behaviour in BTBR mice (Amodeo et al., 2017). Linking that the DMS may be a key region disrupted in BTBR mice which may predispose for excessive RRBI. It is still important to mention that although dysfunction can be observed in the DMS, the connections from the medial prefrontal cortex and the orbitofrontal cortex (OFC) to the DMS may also be a region in the possible modulation of RRBI. Administration of the same 5HT2A receptor antagonist into the OFC has been shown to increase perseveration during reversal learning and enhanced grooming behaviour in BTBR mice (Amodeo et al., 2017). One of characterised neurodevelopmental pathologies have been altered MSN spine density, which are crucially indicative of altered plasticity. In a C58 mouse model of repetitive motor behaviour, decreased spine density was also prominent in the DMS (Curry-Pochy et al., 2020). Furthermore, increased spine density correlated with repetitive motor behaviour (Curry-Pochy et al., 2020). BTBR mice have also been suggested to have a decreased spine density in the DMS (Briones et al., 2021). Furthermore, an injection with chondroitinase ABC (chABC) into the DMS of BTBR mice restored the spine density to that of control mice, and crucially repetitive behaviour such as grooming and digging was alleviated (Briones et al., 2021). These lines of research indicate that additional alterations have been observed in the DMS previously and treatments which do not directly link to PV downregulation directly seem to have a therapeutic effect on the symptoms of RRBI.

4.3 Control mice have a higher percentage of PV+ cells surrounded by PNNs in DLS than DMS

The literature reports that the topographical organisation of PV+ INs is more abundant in the lateral regions of the striatum (Lee et al., 2012). Surprisingly, no difference was found between the DMS and DLS control mice in the density of PV+ INs or the density of PNNs. This lack of gradient of PV+ INs in this study may possibly be due to the selection of ROIs. In

order to maximise the sampling regions and to avoid overlap, DLS ROI were selected slightly more ventral, purely due to the structure of the striatum, to that of the DMS ROI. With there being a higher abundance of PV+ INs in the dorsal compared to the ventral region (Lee et al., 2012), this may explain why no significant difference in PV+ INs was observed. What was found however is that both male and female control mice had a higher % of PV+ INs that colocalised with PNNs in the DLS than in the DMS, which is consistent with the topographical distribution of PV+ INs with PNNs in adult mouse striata described by Lee and colleagues (2012). The importance of PNNs cannot be underestimated, these extracellular matrix structures are not only considered crucial in synaptic plasticity and neuronal maturation, but they may also modulate the neuronal activity of Pvalb INs (Sigal et al., 2019; Carceller et al., 2020). Degradation of PNNs, by injections of chondroitinase ABC (chABC), has been shown to increase the excitability of PV+ INs (Dityatev et al., 2007). Our results show that a greater proportion of PV+ INs are ensheathed with such PNNs in the DLS, which in turn would imply that these INs have decreased excitability. This aligns with electrophysiological results showing that PV+ INs in the DLS of control mice have decreased intrinsic excitability compared to PV+ INs in the DMS region (Monteiro et al., 2018). This paper suggests of a dichotomous population of PV+ INs, of which those in the DLS displayed more extensive arborization and complexity than PV+ INs in the DMS. However, there may not be a dichotomous population as suggested, instead the increasing gradient of colocalisation PV+ INs with PNNs across the DS proceeds to give rise to more mature (Slaker et al., 2016) and less excitable INs in the DLS, which have also been documented to have more extensive arborization and complexity than INs in the DMS (Monteiro et al., 2018). Research also suggests that Pvalb INs surrounded by PNNs are significantly larger than those without PNNs (Aronitz et al., 2021), which may in turn lead to more extensive arborizations and support the findings of Monteiro and colleagues (2018). Although conducted in the hippocampus, research has established that PNNs affect the relative expression of PV, with PV fluorescence being significantly higher in INs with PNNs than in those not ensheathed by PNNs (Yamada et al., 2015). A qRT-PCR analysis also indicated that the digestion of PNNs results in a decrease of PV mRNA (Yamada et al., 2015). This corresponds to the results of Monteiro et al. (2018), which found that PV-immunoreactivity was stronger in the more lateral regions of the striatum compared to the DMS, which in turn corresponds to our findings a higher percentage of VVA+ cells with PV expression in the DLS than in the DMS in the C57 mice. This difference in the percentage of VVA+ cells with PV expression between the DMS and DLS regions may be due to the fact that these regions have different functions in behaviour, therefore the observations

are likely to represent a functional DS which does not predispose control mice to exhibit excessive RRBI. These results further add to the literature which suggest that the medial and lateral regions of the DS have characterised differences.

4.4 Sex differences in BTBR mice - altered colocalisation of PV+ interneurons with perineuronal nets

Control mice display greater percentage of PV+ cells surrounded by VVA in the DLS than in the DMS. In BTBR mice on the other hand, the DMS and DLS regions demonstrated a similar percentage. These results indicate that BTBR mice may have a disruption in functionality between the DMS and DLS regions. These results also reveal that although aetiology is similar, the extent to which PV+ INs are colocalised with PNNs depends on sex of the BTBR mice. This is particularly insightful because previous literature has revealed that female BTBR mice do not exhibit an equal amount of repetitive behaviour to that of male BTBR mice (Amodeo et al., 2019), speculating a neurobiological mechanism through which female mice show a protective effect against the symptoms of RRBI. Briones and colleagues (2021) suggest that BTBR mice have an increased percentage of PV+ cells surrounded by PNNs in the DMS and reducing PNNs alleviates grooming and digging behaviour. Therefore, our observations from female BTBR mice would appear consistent with that of findings Briones and colleagues (2021), although our male BTBR mice did not show such increase. From the conclusions of Briones and colleagues (2021), and the previously established greater RRBI phenotype of male BTBR male compared to females, we would expect that the results of this study would show completely opposite results in the sexes of BTBR mice. With males which we would expect to have much higher percentage of PV+ cells surrounded by PNNs in the DMS and females to possibly show no difference. As to why there may be discrepancies in our results is not easily explainable, however PNN have been shown to be highly plastic and their development is shaped by environmental factors (Carulli & Verhaagen, 2021). The work of Briones and colleagues (2021) has also shown that after almost complete digestion of PNNs by treatment with chABC, density of PNNs is restored to that of baseline after only 10 days post injection. This highlights that examination of single time point may not be as insightful as for example a longitudinal investigation of this colocalisation in BTBR mice, ideally with female BTBR mice to show whether claims of Briones and colleagues (2021) also apply to a model which does not show an identical RRBI phenotype to that of male BTBR mice.

4.5 Limitations and Future Directions

This current study aimed to investigate 8-week-old, adult BTBR mice and hence only the endpoint of ASD aetiology. This study agrees with previous literature adding to the list of mice models of ASD which all exhibit similar pathological alterations, supporting the current evidence that PV downregulation is related to the aetiology of ASD (Filice et al., 2016; Lauber et al., 2016; 2018). However, the decrease in PV levels still remains in question whether it is the causal factor in the aetiology of ASD or whether PV is decreased as a result of another mechanism. ASD is a neurodevelopmental disorder, with alterations that we begin to observe during the course of a child's development. Therefore, a future direction would be to investigate BTBR mice for PV downregulation during early development. This would translate the results of this study into a research of a biomarker for ASD which would possibly allow for an earlier diagnosis in order to make earlier interventions and support individuals which may be predisposed for ASD. This may be possible with BTBR mice with as early as the second postnatal week since aggregations of chondroitin-sulfate proteoglycans (CSPGs), forming the PNNs, begin to emerge in the mouse striatum at postnatal day 10 and continue to increase in density with maturation (Lee et al., 2008). While this would enable to draw conclusions that PV downregulation may be used as a biomarker, it is important to mention that PV expression has been shown to have a close relationship with PNN maturation. It is equally as likely that alterations to the PNNs may be the primary pathology which results in PV reduction. Therefore, another future direction may be to investigate whether alterations in the PNNs also occur during early development.

This study explored alteration in the DS of BTBR mice and aimed to link them to how they may relate to symptoms of RRBI observed in ASD. Unfortunately, behavioural analysis was not part of this study, with only a few studies having examined possible sex differences in the BTBR strain. BTBR mice have been consistently shown to display autism-relevant behaviours, encouraging its use as a tool to research the aetiology of ASD (McFarlane et al., 2008; Bolivar et al., 2007; Moy et al., 2007; Nadler et al., 2006). On the contrary, those which investigated between sexes have revealed that male BTBR mice display social approach, ultrasonic vocalization, marble burying and self-grooming behaviours more than female mice (Amodeo et al., 2019; Schwartz et al., 2013). This study has found that BTBR mice exhibit sex differences in the DS, however complementing such results with a behavioural analysis which shows that behavioural phenotypes differ between the sexes may elucidate the

inconsistencies in the social aspect of male and female BTBR mice but would also permit to make assumptive conclusions that alterations in the DS are responsible for driving RRBI.

Previous literature has already documented that electrophysiological profiles of PV+ INs naturally vary between the DMS and DLS regions in mice (Monteiro et al., 2018), however BTBR mice have not been investigated for this. Therefore, profiling the PV+ INs in the BTBR would transform speculative conclusions of altered E/I balance into evidence-based conclusions. From the results of this study, we can speculate that E/I balance in BTBR mice may be shifted towards increased inhibition due to a reduction of PV in the DMS. Although, we have also observed that the colocalisation of PV+ INs was also altered, which adds to the complexity of PV+ IN function and may mean that any assumptions of E/I balance may be premature without an electrophysiological analysis. Furthermore, it may be more insightful to consider the effect these alterations may have on the greater circuitry of the BG and possibly other regions since in the insular cortex, BTBR mice show decreased mIPSCs frequency in pyramidal cells, in turn suggesting a weakened inhibitory circuitry in this region (Gogolla et al., 2014). Therefore, this indicate that PV reduction in cortical and subcortical regions may surprisingly result in opposing effects on E/I balance.

5.0 CONCLUSION

This study is the first to look into whether PV expression is downregulated in male and female BTBR mice. Additionally, it is the first to investigate sex differences in PNN colocalisation with PV interneurons in the DS subregions of BTBR mice. This study found that BTBR mice, like transgenic and environmental mouse models of ASD, show a decrease of PV in the striata. This PV downregulation in BTBR mice was observed to be accounted by the DMS, which also highlights the importance of studying subregions of the DS. Additional to this, this study found that BTBR mice show alterations in the colocalisation of PV+ INs with PNNs in the DS, with differences between the sexes of BTBR mice. The differences between male and female BTBR mice are in particular insightful since behavioural phenotypes are not exactly the same and ASD behaviours are more exhibited by male counterparts. Through further research, it may be possible to determine the effect of complex interaction between PV reduction and alterations in the colocalisation of PV+ INs with PNNs within the DS on E/I balance and whether this may be responsible for symptoms of RRBI observed in BTBR mice models of idiopathic ASD.

6.0 REFERENCES

- American Psychiatric Association (2013). *Diagnostic and statistical manual of mental disorders*. <https://doi.org/10.1176/appi.books.9780890425596>
- Amodeo, D. A., Jones, J. H., Sweeney, J. A., & Ragozzino, M. E. (2012). Differences in BTBR T+ tf/J and C57BL/6J mice on probabilistic reversal learning and stereotyped behaviors. *Behavioural brain research*, 227(1), 64–72. <https://doi.org/10.1016/j.bbr.2011.10.032>
- Amodeo, D. A., Pahua, A. E., Zarate, M., Taylor, J. A., Peterson, S., Posadas, R., Oliver, B. L., & Amodeo, L. R. (2019). Differences in the expression of restricted repetitive behaviors in female and male BTBR T+ tf/J mice. *Behavioural brain research*, 372, 112028. <https://doi.org/10.1016/j.bbr.2019.112028>
- Amodeo, D. A., Rivera, E., Cook, E. H., Jr, Sweeney, J. A., & Ragozzino, M. E. (2017). 5HT_{2A} receptor blockade in dorsomedial striatum reduces repetitive behaviors in BTBR mice. *Genes, brain, and behavior*, 16(3), 342–351. <https://doi.org/10.1111/gbb.12343>
- Andrews, D. S., Aksman, L., Kerns, C. M., Lee, J. K., Winder-Patel, B. M., Harvey, D. J., Waizbard-Bartov, E., Heath, B., Solomon, M., Rogers, S. J., Altmann, A., Nordahl, C. W., & Amaral, D. G. (2022). Association of Amygdala Development With Different Forms of Anxiety in Autism Spectrum Disorder. *Biological psychiatry*, 91(11), 977–987. <https://doi.org/10.1016/j.biopsych.2022.01.016>
- Ariza, J., Rogers, H., Hashemi, E., Noctor, S. C., & Martínez-Cerdeño, V. (2018). The Number of Chandelier and Basket Cells Are Differentially Decreased in Prefrontal Cortex in Autism. *Cerebral cortex (New York, N.Y. : 1991)*, 28(2), 411–420. <https://doi.org/10.1093/cercor/bhw349>
- Aronitz, E. M., Kamermans, B. A., & Duffy, K. R. (2021). Development of parvalbumin neurons and perineuronal nets in the visual cortex of normal and dark-exposed cats. *The Journal of comparative neurology*, 529(11), 2827–2841. <https://doi.org/10.1002/cne.25127>
- Balleine, B. W., Delgado, M. R., & Hikosaka, O. (2007). The role of the dorsal striatum in reward and decision-making. *The Journal of neuroscience : the official journal of the Society for Neuroscience*, 27(31), 8161–8165. <https://doi.org/10.1523/JNEUROSCI.1554-07.2007>
- Balleine, B. W., Liljeholm, M., & Ostlund, S. B. (2009). The integrative function of the basal ganglia in instrumental conditioning. *Behavioural brain research*, 199(1), 43–52. <https://doi.org/10.1016/j.bbr.2008.10.034>
- Bennett, B. D., & Bolam, J. P. (1993). Characterization of calretinin-immunoreactive structures in the striatum of the rat. *Brain research*, 609(1-2), 137–148. [https://doi.org/10.1016/0006-8993\(93\)90866-1](https://doi.org/10.1016/0006-8993(93)90866-1)

- Bolivar, V. J., Walters, S. R., & Phoenix, J. L. (2007). Assessing autism-like behavior in mice: variations in social interactions among inbred strains. *Behavioural brain research*, 176(1), 21–26. <https://doi.org/10.1016/j.bbr.2006.09.007>
- Briones, B. A., Pitcher, M. N., Fleming, W. T., Libby, A., Diethorn, E. J., Haye, A. E., MacDowell, C. J., Zych, A. D., Waters, R. C., Buschman, T. J., Witten, I. B., & Gould, E. (2021). Perineuronal Nets in the Dorsomedial Striatum Contribute to Behavioral Dysfunction in Mouse Models of Excessive Repetitive Behavior. *Biological psychiatry global open science*, 2(4), 460–469. <https://doi.org/10.1016/j.bpsgos.2021.11.005>
- Caillard, O., Moreno, H., Schwaller, B., Llano, I., Celio, M. R., & Marty, A. (2000). Role of the calcium-binding protein parvalbumin in short-term synaptic plasticity. *Proceedings of the National Academy of Sciences of the United States of America*, 97(24), 13372–13377. <https://doi.org/10.1073/pnas.230362997>
- Calderoni, S., Bellani, M., Hardan, A. Y., Muratori, F., & Brambilla, P. (2014). Basal ganglia and restricted and repetitive behaviours in Autism Spectrum Disorders: current status and future perspectives. *Epidemiology and psychiatric sciences*, 23(3), 235–238. <https://doi.org/10.1017/S2045796014000171>
- Carceller, H., Guirado, R., Ripolles-Campos, E., Teruel-Marti, V., & Nacher, J. (2020). Perineuronal Nets Regulate the Inhibitory Perisomatic Input onto Parvalbumin Interneurons and γ Activity in the Prefrontal Cortex. *The Journal of neuroscience : the official journal of the Society for Neuroscience*, 40(26), 5008–5018. <https://doi.org/10.1523/JNEUROSCI.0291-20.2020>
- Carulli, D., & Verhaagen, J. (2021). An Extracellular Perspective on CNS Maturation: Perineuronal Nets and the Control of Plasticity. *International journal of molecular sciences*, 22(5), 2434. <https://doi.org/10.3390/ijms22052434>
- Casanova, M. F., Casanova, E. L., Frye, R. E., Baeza-Velasco, C., LaSalle, J. M., Hagerman, R. J., Scherer, S. W., & Natowicz, M. R. (2020). Editorial: Secondary vs. Idiopathic Autism. *Frontiers in psychiatry*, 11, 297. <https://doi.org/10.3389/fpsy.2020.00297>
- Chesselet, M. F., & Graybiel, A. M. (1986). Striatal neurons expressing somatostatin-like immunoreactivity: evidence for a peptidergic interneuronal system in the cat. *Neuroscience*, 17(3), 547–571. [https://doi.org/10.1016/0306-4522\(86\)90030-8](https://doi.org/10.1016/0306-4522(86)90030-8)
- Corbit, L. H., Leung, B. K., & Balleine, B. W. (2013). The role of the amygdala-striatal pathway in the acquisition and performance of goal-directed instrumental actions. *The Journal of neuroscience : the official journal of the Society for Neuroscience*, 33(45), 17682–17690. <https://doi.org/10.1523/JNEUROSCI.3271-13.2013>
- Courchesne, E., Campbell, K., & Solso, S. (2011). Brain growth across the life span in autism: age-specific changes in anatomical pathology. *Brain research*, 1380, 138–145. <https://doi.org/10.1016/j.brainres.2010.09.101>
- Cowan, R. L., Wilson, C. J., Emson, P. C., & Heizmann, C. W. (1990). Parvalbumin-containing GABAergic interneurons in the rat neostriatum. *The Journal of comparative neurology*, 302(2), 197–205. <https://doi.org/10.1002/cne.903020202>

- Cragg, S. J., Hille, C. J., & Greenfield, S. A. (2002). Functional domains in dorsal striatum of the nonhuman primate are defined by the dynamic behavior of dopamine. *The Journal of neuroscience : the official journal of the Society for Neuroscience*, 22(13), 5705–5712. <https://doi.org/10.1523/JNEUROSCI.22-13-05705.2002>
- Crawley J. N. (2012). Translational animal models of autism and neurodevelopmental disorders. *Dialogues in clinical neuroscience*, 14(3), 293–305. <https://doi.org/10.31887/DCNS.2012.14.3/jcrawley>
- Curry-Pochy, L. S., Kravetz, Z., Feinstein, J., Yaffe, B., Tanios, V., Makar, J., & Lewis, M. H. (2020). Differential consequences of habitual responding in a mouse model of repetitive behavior. *Behavioral neuroscience*, 134(1), 21–33. <https://doi.org/10.1037/bne0000348>
- Defensor, E. B., Pearson, B. L., Pobbe, R. L., Bolivar, V. J., Blanchard, D. C., & Blanchard, R. J. (2011). A novel social proximity test suggests patterns of social avoidance and gaze aversion-like behavior in BTBR T+ tf/J mice. *Behavioural brain research*, 217(2), 302–308. <https://doi.org/10.1016/j.bbr.2010.10.033>
- Dityatev, A., Brückner, G., Dityateva, G., Grosche, J., Kleene, R., & Schachner, M. (2007). Activity-dependent formation and functions of chondroitin sulfate-rich extracellular matrix of perineuronal nets. *Developmental neurobiology*, 67(5), 570–588. <https://doi.org/10.1002/dneu.20361>
- Estes, A., Shaw, D. W., Sparks, B. F., Friedman, S., Giedd, J. N., Dawson, G., Bryan, M., & Dager, S. R. (2011). Basal ganglia morphometry and repetitive behavior in young children with autism spectrum disorder. *Autism research : official journal of the International Society for Autism Research*, 4(3), 212–220. <https://doi.org/10.1002/aur.193>
- Fatemi, S. H., Halt, A. R., Stary, J. M., Kanodia, R., Schulz, S. C., & Realmuto, G. R. (2002). Glutamic acid decarboxylase 65 and 67 kDa proteins are reduced in autistic parietal and cerebellar cortices. *Biological psychiatry*, 52(8), 805–810. [https://doi.org/10.1016/s0006-3223\(02\)01430-0](https://doi.org/10.1016/s0006-3223(02)01430-0)
- Fatemi, S. H., Reutiman, T. J., Folsom, T. D., & Thuras, P. D. (2009). GABA(A) receptor downregulation in brains of subjects with autism. *Journal of autism and developmental disorders*, 39(2), 223–230. <https://doi.org/10.1007/s10803-008-0646-7>
- Ferguson, B. R., & Gao, W. J. (2018). PV Interneurons: Critical Regulators of E/I Balance for Prefrontal Cortex-Dependent Behavior and Psychiatric Disorders. *Frontiers in neural circuits*, 12, 37. <https://doi.org/10.3389/fncir.2018.00037>
- Filice, F., Janickova, L., Henzi, T., Bilella, A., & Schwaller, B. (2020). The Parvalbumin Hypothesis of Autism Spectrum Disorder. *Frontiers in cellular neuroscience*, 14, 577525. <https://doi.org/10.3389/fncel.2020.577525>
- Filice, F., Lauber, E., Vörckel, K. J., Wöhr, M., & Schwaller, B. (2018). 17- β estradiol increases parvalbumin levels in *Pvalb* heterozygous mice and attenuates behavioral phenotypes with relevance to autism core symptoms. *Molecular autism*, 9, 15. <https://doi.org/10.1186/s13229-018-0199-3>

- Filice, F., Vörckel, K. J., Sungur, A. Ö., Wöhr, M., & Schwaller, B. (2016). Reduction in parvalbumin expression not loss of the parvalbumin-expressing GABA interneuron subpopulation in genetic parvalbumin and shank mouse models of autism. *Molecular brain*, 9, 10. <https://doi.org/10.1186/s13041-016-0192-8>
- Fuccillo M. V. (2016). Striatal Circuits as a Common Node for Autism Pathophysiology. *Frontiers in neuroscience*, 10, 27. <https://doi.org/10.3389/fnins.2016.00027>
- Gerfen, C. R., Engber, T. M., Mahan, L. C., Susel, Z., Chase, T. N., Monsma, F. J., Jr, & Sibley, D. R. (1990). D1 and D2 dopamine receptor-regulated gene expression of striatonigral and striatopallidal neurons. *Science (New York, N.Y.)*, 250(4986), 1429–1432. <https://doi.org/10.1126/science.2147780>
- Gogolla, N., Leblanc, J. J., Quast, K. B., Südhof, T. C., Fagiolini, M., & Hensch, T. K. (2009). Common circuit defect of excitatory-inhibitory balance in mouse models of autism. *Journal of neurodevelopmental disorders*, 1(2), 172–181. <https://doi.org/10.1007/s11689-009-9023-x>
- Gogolla, N., Takesian, A. E., Feng, G., Fagiolini, M., & Hensch, T. K. (2014). Sensory integration in mouse insular cortex reflects GABA circuit maturation. *Neuron*, 83(4), 894–905. <https://doi.org/10.1016/j.neuron.2014.06.033>
- Graybiel A. M. (2008). Habits, rituals, and the evaluative brain. *Annual review of neuroscience*, 31, 359–387. <https://doi.org/10.1146/annurev.neuro.29.051605.112851>
- Graybiel, A. M., & Grafton, S. T. (2015). The striatum: where skills and habits meet. *Cold Spring Harbor perspectives in biology*, 7(8), a021691. <https://doi.org/10.1101/cshperspect.a021691>
- Griffiths, K. R., Morris, R. W., & Balleine, B. W. (2014). Translational studies of goal-directed action as a framework for classifying deficits across psychiatric disorders. *Frontiers in systems neuroscience*, 8, 101. <https://doi.org/10.3389/fnsys.2014.00101>
- Guptill, J. T., Booker, A. B., Gibbs, T. T., Kemper, T. L., Bauman, M. L., & Blatt, G. J. (2007). [3H]-flunitrazepam-labeled benzodiazepine binding sites in the hippocampal formation in autism: a multiple concentration autoradiographic study. *Journal of autism and developmental disorders*, 37(5), 911–920. <https://doi.org/10.1007/s10803-006-0226-7>
- Han, S., Tai, C., Jones, C. J., Scheuer, T., & Catterall, W. A. (2014). Enhancement of inhibitory neurotransmission by GABAA receptors having $\alpha 2,3$ -subunits ameliorates behavioral deficits in a mouse model of autism. *Neuron*, 81(6), 1282–1289. <https://doi.org/10.1016/j.neuron.2014.01.016>
- Hardan, A. Y., Kilpatrick, M., Keshavan, M. S., & Minshew, N. J. (2003). Motor performance and anatomic magnetic resonance imaging (MRI) of the basal ganglia in autism. *Journal of child neurology*, 18(5), 317–324. <https://doi.org/10.1177/08830738030180050801>
- Härtig, W., Derouiche, A., Welt, K., Brauer, K., Grosche, J., Mäder, M., Reichenbach, A., & Brückner, G. (1999). Cortical neurons immunoreactive for the potassium channel Kv3.1b subunit are predominantly surrounded by perineuronal nets presumed as a

- buffering system for cations. *Brain research*, 842(1), 15–29.
[https://doi.org/10.1016/s0006-8993\(99\)01784-9](https://doi.org/10.1016/s0006-8993(99)01784-9)
- Härtig, W., Meinicke, A., Michalski, D., Schob, S., & Jäger, C. (2022). Update on Perineuronal Net Staining With *Wisteria floribunda* Agglutinin (WFA). *Frontiers in integrative neuroscience*, 16, 851988. <https://doi.org/10.3389/fnint.2022.851988>
- Hashemi, E., Ariza, J., Rogers, H., Noctor, S. C., & Martínez-Cerdeño, V. (2018). The Number of Parvalbumin-Expressing Interneurons Is Decreased in the Prefrontal Cortex in Autism. *Cerebral cortex (New York, N.Y. : 1991)*, 28(2), 690.
<https://doi.org/10.1093/cercor/bhx063>
- Hattier, M. A., Matson, J. L., Tureck, K., & Horovitz, M. (2011). The effects of gender and age on repetitive and/or restricted behaviors and interests in adults with autism spectrum disorders and intellectual disability. *Research in developmental disabilities*, 32(6), 2346–2351. <https://doi.org/10.1016/j.ridd.2011.07.028>
- Hollander, E., Anagnostou, E., Chaplin, W., Esposito, K., Haznedar, M. M., Licalzi, E., Wasserman, S., Soorya, L., & Buchsbaum, M. (2005). Striatal volume on magnetic resonance imaging and repetitive behaviors in autism. *Biological psychiatry*, 58(3), 226–232. <https://doi.org/10.1016/j.biopsych.2005.03.040>
- Howard, M. W., Rizzuto, D. S., Caplan, J. B., Madsen, J. R., Lisman, J., Aschenbrenner-Scheibe, R., Schulze-Bonhage, A., & Kahana, M. J. (2003). Gamma oscillations correlate with working memory load in humans. *Cerebral cortex (New York, N.Y. : 1991)*, 13(12), 1369–1374. <https://doi.org/10.1093/cercor/bhg084>
- Hutsler, J. J., & Zhang, H. (2010). Increased dendritic spine densities on cortical projection neurons in autism spectrum disorders. *Brain research*, 1309, 83–94.
<https://doi.org/10.1016/j.brainres.2009.09.120>
- Iossifov, I., O’Roak, B. J., Sanders, S. J., Ronemus, M., Krumm, N., Levy, D., Stessman, H. A., Witherspoon, K. T., Vives, L., Patterson, K. E., Smith, J. D., Paeper, B., Nickerson, D. A., Dea, J., Dong, S., Gonzalez, L. E., Mandell, J. D., Mane, S. M., Murtha, M. T., Sullivan, C. A., ... Wigler, M. (2014). The contribution of de novo coding mutations to autism spectrum disorder. *Nature*, 515(7526), 216–221.
<https://doi.org/10.1038/nature13908>
- Kawaguchi, Y., & Kubota, Y. (1997). GABAergic cell subtypes and their synaptic connections in rat frontal cortex. *Cerebral cortex (New York, N.Y. : 1991)*, 7(6), 476–486. <https://doi.org/10.1093/cercor/7.6.476>
- Kawaguchi, Y., Katsumaru, H., Kosaka, T., Heizmann, C. W., & Hama, K. (1987). Fast spiking cells in rat hippocampus (CA1 region) contain the calcium-binding protein parvalbumin. *Brain research*, 416(2), 369–374. [https://doi.org/10.1016/0006-8993\(87\)90921-8](https://doi.org/10.1016/0006-8993(87)90921-8)
- Kawaguchi, Y., Wilson, C. J., Augood, S. J., & Emson, P. C. (1995). Striatal interneurons: chemical, physiological and morphological characterization. *Trends in neurosciences*, 18(12), 527–535. [https://doi.org/10.1016/0166-2236\(95\)98374-8](https://doi.org/10.1016/0166-2236(95)98374-8)

- Kelley, A. E., Domesick, V. B., & Nauta, W. J. (1982). The amygdalostriatal projection in the rat--an anatomical study by anterograde and retrograde tracing methods. *Neuroscience*, 7(3), 615–630. [https://doi.org/10.1016/0306-4522\(82\)90067-7](https://doi.org/10.1016/0306-4522(82)90067-7)
- Kita, H., Kosaka, T., & Heizmann, C. W. (1990). Parvalbumin-immunoreactive neurons in the rat neostriatum: a light and electron microscopic study. *Brain research*, 536(1-2), 1–15. [https://doi.org/10.1016/0006-8993\(90\)90002-s](https://doi.org/10.1016/0006-8993(90)90002-s)
- Kohls, G., Yerys, B. E., & Schultz, R. T. (2014). Striatal development in autism: repetitive behaviors and the reward circuitry. *Biological psychiatry*, 76(5), 358–359. <https://doi.org/10.1016/j.biopsych.2014.07.010>
- Koós, T., & Tepper, J. M. (1999). Inhibitory control of neostriatal projection neurons by GABAergic interneurons. *Nature neuroscience*, 2(5), 467–472. <https://doi.org/10.1038/8138>
- Kreitzer A. C. (2009). Physiology and pharmacology of striatal neurons. *Annual review of neuroscience*, 32, 127–147. <https://doi.org/10.1146/annurev.neuro.051508.135422>
- Lanciego, J. L., Luquin, N., & Obeso, J. A. (2012). Functional neuroanatomy of the basal ganglia. *Cold Spring Harbor perspectives in medicine*, 2(12), a009621. <https://doi.org/10.1101/cshperspect.a009621>
- Langen, M., Bos, D., Noordermeer, S. D., Nederveen, H., van Engeland, H., & Durston, S. (2014). Changes in the development of striatum are involved in repetitive behavior in autism. *Biological psychiatry*, 76(5), 405–411. <https://doi.org/10.1016/j.biopsych.2013.08.013>
- Langen, M., Durston, S., Staal, W. G., Palmen, S. J., & van Engeland, H. (2007). Caudate nucleus is enlarged in high-functioning medication-naive subjects with autism. *Biological psychiatry*, 62(3), 262–266. <https://doi.org/10.1016/j.biopsych.2006.09.040>
- Lauber, E., Filice, F., & Schwaller, B. (2016). Prenatal Valproate Exposure Differentially Affects Parvalbumin-Expressing Neurons and Related Circuits in the Cortex and Striatum of Mice. *Frontiers in molecular neuroscience*, 9, 150. <https://doi.org/10.3389/fnmol.2016.00150>
- Lauber, E., Filice, F., & Schwaller, B. (2018). Dysregulation of Parvalbumin Expression in the *Cntnap2*^{-/-} Mouse Model of Autism Spectrum Disorder. *Frontiers in molecular neuroscience*, 11, 262. <https://doi.org/10.3389/fnmol.2018.00262>
- Lee, H., Leamey, C. A., & Sawatari, A. (2008). Rapid reversal of chondroitin sulfate proteoglycan associated staining in subcompartments of mouse neostriatum during the emergence of behaviour. *PloS one*, 3(8), e3020. <https://doi.org/10.1371/journal.pone.0003020>
- Lee, H., Leamey, C. A., & Sawatari, A. (2012). Perineuronal nets play a role in regulating striatal function in the mouse. *PloS one*, 7(3), e32747. <https://doi.org/10.1371/journal.pone.0032747>

- Lewis, D. A., Curley, A. A., Glausier, J. R., & Volk, D. W. (2012). Cortical parvalbumin interneurons and cognitive dysfunction in schizophrenia. *Trends in neurosciences*, 35(1), 57–67. <https://doi.org/10.1016/j.tins.2011.10.004>
- Lipton, D. M., Gonzales, B. J., & Citri, A. (2019). Dorsal Striatal Circuits for Habits, Compulsions and Addictions. *Frontiers in systems neuroscience*, 13, 28. <https://doi.org/10.3389/fnsys.2019.00028>
- Loomes, R., Hull, L., & Mandy, W. P. L. (2017). What Is the Male-to-Female Ratio in Autism Spectrum Disorder? A Systematic Review and Meta-Analysis. *Journal of the American Academy of Child and Adolescent Psychiatry*, 56(6), 466–474. <https://doi.org/10.1016/j.jaac.2017.03.013>
- Lovinger, D.M. & Mathur, B.N. (2016) ‘Endocannabinoid signaling in the striatum’, *Handbook of Behavioral Neuroscience*, pp. 197–215. doi:10.1016/b978-0-12-802206-1.00010-6.
- Maenner, M. J., Shaw, K. A., Bakian, A. V., Bilder, D. A., Durkin, M. S., Esler, A., Furnier, S. M., Hallas, L., Hall-Lande, J., Hudson, A., Hughes, M. M., Patrick, M., Pierce, K., Poynter, J. N., Salinas, A., Shenouda, J., Vehorn, A., Warren, Z., Constantino, J. N., DiRienzo, M., ... Cogswell, M. E. (2021). Prevalence and Characteristics of Autism Spectrum Disorder Among Children Aged 8 Years - Autism and Developmental Disabilities Monitoring Network, 11 Sites, United States, 2018. *Morbidity and mortality weekly report. Surveillance summaries (Washington, D.C. : 2002)*, 70(11), 1–16. <https://doi.org/10.15585/mmwr.ss7011a1>
- Mandy, W., Chilvers, R., Chowdhury, U., Salter, G., Seigal, A., & Skuse, D. (2012). Sex differences in autism spectrum disorder: evidence from a large sample of children and adolescents. *Journal of autism and developmental disorders*, 42(7), 1304–1313. <https://doi.org/10.1007/s10803-011-1356-0>
- McFarlane, H. G., Kusek, G. K., Yang, M., Phoenix, J. L., Bolivar, V. J., & Crawley, J. N. (2008). Autism-like behavioral phenotypes in BTBR T+tf/J mice. *Genes, brain, and behavior*, 7(2), 152–163. <https://doi.org/10.1111/j.1601-183X.2007.00330.x>
- Menzies, L., Chamberlain, S. R., Laird, A. R., Thelen, S. M., Sahakian, B. J., & Bullmore, E. T. (2008). Integrating evidence from neuroimaging and neuropsychological studies of obsessive-compulsive disorder: the orbitofronto-striatal model revisited. *Neuroscience and biobehavioral reviews*, 32(3), 525–549. <https://doi.org/10.1016/j.neubiorev.2007.09.005>
- Meyza, K. Z., & Blanchard, D. C. (2017). The BTBR mouse model of idiopathic autism - Current view on mechanisms. *Neuroscience and biobehavioral reviews*, 76(Pt A), 99–110. <https://doi.org/10.1016/j.neubiorev.2016.12.037>
- Monteiro, P., Barak, B., Zhou, Y., McRae, R., Rodrigues, D., Wickersham, I. R., & Feng, G. (2018). Dichotomous parvalbumin interneuron populations in dorsolateral and dorsomedial striatum. *The Journal of physiology*, 596(16), 3695–3707. <https://doi.org/10.1113/JP275936>

- Moy, S. S., Nadler, J. J., Young, N. B., Perez, A., Holloway, L. P., Barbaro, R. P., Barbaro, J. R., Wilson, L. M., Threadgill, D. W., Lauder, J. M., Magnuson, T. R., & Crawley, J. N. (2007). Mouse behavioral tasks relevant to autism: phenotypes of 10 inbred strains. *Behavioural brain research*, *176*(1), 4–20. <https://doi.org/10.1016/j.bbr.2006.07.030>
- Müller, M., Felmy, F., Schwaller, B., & Schneggenburger, R. (2007). Parvalbumin is a mobile presynaptic Ca²⁺ buffer in the calyx of Held that accelerates the decay of Ca²⁺ and short-term facilitation. *The Journal of neuroscience : the official journal of the Society for Neuroscience*, *27*(9), 2261–2271. <https://doi.org/10.1523/JNEUROSCI.5582-06.2007>
- Nadler, J. J., Zou, F., Huang, H., Moy, S. S., Lauder, J., Crawley, J. N., Threadgill, D. W., Wright, F. A., & Magnuson, T. R. (2006). Large-scale gene expression differences across brain regions and inbred strains correlate with a behavioral phenotype. *Genetics*, *174*(3), 1229–1236. <https://doi.org/10.1534/genetics.106.061481>
- Nahar, L., Delacroix, B. M., & Nam, H. W. (2021). The Role of Parvalbumin Interneurons in Neurotransmitter Balance and Neurological Disease. *Frontiers in psychiatry*, *12*, 679960. <https://doi.org/10.3389/fpsyt.2021.679960>
- Oblak, A. L., Gibbs, T. T., & Blatt, G. J. (2010). Decreased GABA(B) receptors in the cingulate cortex and fusiform gyrus in autism. *Journal of neurochemistry*, *114*(5), 1414–1423. <https://doi.org/10.1111/j.1471-4159.2010.06858.x>
- O'Hare, J. K., Li, H., Kim, N., Gaidis, E., Ade, K., Beck, J., Yin, H., & Calakos, N. (2017). Striatal fast-spiking interneurons selectively modulate circuit output and are required for habitual behavior. *eLife*, *6*, e26231. <https://doi.org/10.7554/eLife.26231>
- Orduz, D., Bishop, D. P., Schwaller, B., Schiffmann, S. N., & Gall, D. (2013). Parvalbumin tunes spike-timing and efferent short-term plasticity in striatal fast spiking interneurons. *The Journal of physiology*, *591*(13), 3215–3232. <https://doi.org/10.1113/jphysiol.2012.250795>
- Parikshak, N. N., Luo, R., Zhang, A., Won, H., Lowe, J. K., Chandran, V., Horvath, S., & Geschwind, D. H. (2013). Integrative functional genomic analyses implicate specific molecular pathways and circuits in autism. *Cell*, *155*(5), 1008–1021. <https://doi.org/10.1016/j.cell.2013.10.031>
- Paxinos, G. & Franklin, K. (2007). *The Mouse Brain in Stereotaxic Coordinates*. 3rd ed. New York: Elsevier/Academic Press.
- Ragozzino, M. E., Ragozzino, K. E., Mizumori, S. J., & Kesner, R. P. (2002). Role of the dorsomedial striatum in behavioral flexibility for response and visual cue discrimination learning. *Behavioral neuroscience*, *116*(1), 105–115. <https://doi.org/10.1037//0735-7044.116.1.105>
- Roessner, V., Overlack, S., Schmidt-Samoa, C., Baudewig, J., Dechent, P., Rothenberger, A., & Helms, G. (2011). Increased putamen and callosal motor subregion in treatment-naïve boys with Tourette syndrome indicates changes in the bihemispheric motor

- network. *Journal of child psychology and psychiatry, and allied disciplines*, 52(3), 306–314. <https://doi.org/10.1111/j.1469-7610.2010.02324.x>
- Rubenstein, J. L., & Merzenich, M. M. (2003). Model of autism: increased ratio of excitation/inhibition in key neural systems. *Genes, brain, and behavior*, 2(5), 255–267. <https://doi.org/10.1034/j.1601-183x.2003.00037.x>
- Sato, W., Kubota, Y., Kochiyama, T., Uono, S., Yoshimura, S., Sawada, R., Sakihama, M., & Toichi, M. (2014). Increased putamen volume in adults with autism spectrum disorder. *Frontiers in human neuroscience*, 8, 957. <https://doi.org/10.3389/fnhum.2014.00957>
- Scattoni, M. L., Ricceri, L., & Crawley, J. N. (2011). Unusual repertoire of vocalizations in adult BTBR T+tf/J mice during three types of social encounters. *Genes, brain, and behavior*, 10(1), 44–56. <https://doi.org/10.1111/j.1601-183X.2010.00623.x>
- Schaafsma, S. M., & Pfaff, D. W. (2014). Etiologies underlying sex differences in Autism Spectrum Disorders. *Frontiers in neuroendocrinology*, 35(3), 255–271. <https://doi.org/10.1016/j.yfrne.2014.03.006>
- Schwartz, J. J., Careaga, M., Onore, C. E., Rushakoff, J. A., Berman, R. F., & Ashwood, P. (2013). Maternal immune activation and strain specific interactions in the development of autism-like behaviors in mice. *Translational psychiatry*, 3(3), e240. <https://doi.org/10.1038/tp.2013.16>
- Schwede, M., Nagpal, S., Gandal, M. J., Parikshak, N. N., Mirnics, K., Geschwind, D. H., & Morrow, E. M. (2018). Strong correlation of downregulated genes related to synaptic transmission and mitochondria in post-mortem autism cerebral cortex. *Journal of neurodevelopmental disorders*, 10(1), 18. <https://doi.org/10.1186/s11689-018-9237-x>
- Sears, L. L., Vest, C., Mohamed, S., Bailey, J., Ranson, B. J., & Piven, J. (1999). An MRI study of the basal ganglia in autism. *Progress in neuro-psychopharmacology & biological psychiatry*, 23(4), 613–624. [https://doi.org/10.1016/s0278-5846\(99\)00020-2](https://doi.org/10.1016/s0278-5846(99)00020-2)
- Selten, M., van Bokhoven, H., & Nadif Kasri, N. (2018). Inhibitory control of the excitatory/inhibitory balance in psychiatric disorders. *F1000Research*, 7, 23. <https://doi.org/10.12688/f1000research.12155.1>
- Shigematsu, N., Nishi, A., & Fukuda, T. (2019). Gap Junctions Interconnect Different Subtypes of Parvalbumin-Positive Interneurons in Barrels and Septa with Connectivity Unique to Each Subtype. *Cerebral cortex (New York, N.Y. : 1991)*, 29(4), 1414–1429. <https://doi.org/10.1093/cercor/bhy038>
- Sigal, Y. M., Bae, H., Bogart, L. J., Hensch, T. K., & Zhuang, X. (2019). Structural maturation of cortical perineuronal nets and their perforating synapses revealed by superresolution imaging. *Proceedings of the National Academy of Sciences of the United States of America*, 116(14), 7071–7076. <https://doi.org/10.1073/pnas.1817222116>

- Slaker, M. L., Harkness, J. H., & Sorg, B. A. (2016). A standardized and automated method of perineuronal net analysis using *Wisteria floribunda* agglutinin staining intensity. *IBRO reports*, *1*, 54–60. <https://doi.org/10.1016/j.ibror.2016.10.001>
- Snijders, T. M., Milivojevic, B., & Kemner, C. (2013). Atypical excitation-inhibition balance in autism captured by the gamma response to contextual modulation. *NeuroImage. Clinical*, *3*, 65–72. <https://doi.org/10.1016/j.nicl.2013.06.015>
- Solomon, M., Miller, M., Taylor, S. L., Hinshaw, S. P., & Carter, C. S. (2012). Autism symptoms and internalizing psychopathology in girls and boys with autism spectrum disorders. *Journal of autism and developmental disorders*, *42*(1), 48–59. <https://doi.org/10.1007/s10803-011-1215-z>
- Stephenson, D. T., O'Neill, S. M., Narayan, S., Tiwari, A., Arnold, E., Samaroo, H. D., Du, F., Ring, R. H., Campbell, B., Pletcher, M., Vaidya, V. A., & Morton, D. (2011). Histopathologic characterization of the BTBR mouse model of autistic-like behavior reveals selective changes in neurodevelopmental proteins and adult hippocampal neurogenesis. *Molecular autism*, *2*(1), 7. <https://doi.org/10.1186/2040-2392-2-7>
- Sun, L., Grützner, C., Bölte, S., Wibrals, M., Tozman, T., Schlitt, S., Poustka, F., Singer, W., Freitag, C. M., & Uhlhaas, P. J. (2012). Impaired gamma-band activity during perceptual organization in adults with autism spectrum disorders: evidence for dysfunctional network activity in frontal-posterior cortices. *The Journal of neuroscience : the official journal of the Society for Neuroscience*, *32*(28), 9563–9573. <https://doi.org/10.1523/JNEUROSCI.1073-12.2012>
- Szatmari, P., Liu, X. Q., Goldberg, J., Zwaigenbaum, L., Paterson, A. D., Woodbury-Smith, M., Georgiades, S., Duku, E., & Thompson, A. (2012). Sex differences in repetitive stereotyped behaviors in autism: implications for genetic liability. *American journal of medical genetics. Part B, Neuropsychiatric genetics : the official publication of the International Society of Psychiatric Genetics*, *159B*(1), 5–12. <https://doi.org/10.1002/ajmg.b.31238>
- Tepper, J. M., & Bolam, J. P. (2004). Functional diversity and specificity of neostriatal interneurons. *Current opinion in neurobiology*, *14*(6), 685–692. <https://doi.org/10.1016/j.conb.2004.10.003>
- Tepper, J. M., Koós, T., & Wilson, C. J. (2004). GABAergic microcircuits in the neostriatum. *Trends in neurosciences*, *27*(11), 662–669. <https://doi.org/10.1016/j.tins.2004.08.007>
- Vincent, S. R., Johansson, O., Hökfelt, T., Skirboll, L., Elde, R. P., Terenius, L., Kimmel, J., & Goldstein, M. (1983). NADPH-diaphorase: a selective histochemical marker for striatal neurons containing both somatostatin- and avian pancreatic polypeptide (APP)-like immunoreactivities. *The Journal of comparative neurology*, *217*(3), 252–263. <https://doi.org/10.1002/cne.902170303>
- Voineagu, I., Wang, X., Johnston, P., Lowe, J. K., Tian, Y., Horvath, S., Mill, J., Cantor, R. M., Blencowe, B. J., & Geschwind, D. H. (2011). Transcriptomic analysis of autistic brain reveals convergent molecular pathology. *Nature*, *474*(7351), 380–384. <https://doi.org/10.1038/nature10110>

- Voorn, P., Vanderschuren, L. J., Groenewegen, H. J., Robbins, T. W., & Pennartz, C. M. (2004). Putting a spin on the dorsal-ventral divide of the striatum. *Trends in neurosciences*, 27(8), 468–474. <https://doi.org/10.1016/j.tins.2004.06.006>
- Werling, D. M., & Geschwind, D. H. (2013). Sex differences in autism spectrum disorders. *Current opinion in neurology*, 26(2), 146–153. <https://doi.org/10.1097/WCO.0b013e32835ee548>
- Weston C. S. E. (2019). Four Social Brain Regions, Their Dysfunctions, and Sequelae, Extensively Explain Autism Spectrum Disorder Symptomatology. *Brain sciences*, 9(6), 130. <https://doi.org/10.3390/brainsci9060130>
- Wilson, T. W., Rojas, D. C., Reite, M. L., Teale, P. D., & Rogers, S. J. (2007). Children and adolescents with autism exhibit reduced MEG steady-state gamma responses. *Biological psychiatry*, 62(3), 192–197. <https://doi.org/10.1016/j.biopsych.2006.07.002>
- Wöhr, M., Orduz, D., Gregory, P., Moreno, H., Khan, U., Vörckel, K. J., Wolfer, D. P., Welzl, H., Gall, D., Schiffmann, S. N., & Schwaller, B. (2015). Lack of parvalbumin in mice leads to behavioral deficits relevant to all human autism core symptoms and related neural morphofunctional abnormalities. *Translational psychiatry*, 5(3), e525. <https://doi.org/10.1038/tp.2015.19>
- Wöhr, M., Orduz, D., Gregory, P., Moreno, H., Khan, U., Vörckel, K. J., Wolfer, D. P., Welzl, H., Gall, D., Schiffmann, S. N., & Schwaller, B. (2015). Lack of parvalbumin in mice leads to behavioral deficits relevant to all human autism core symptoms and related neural morphofunctional abnormalities. *Translational psychiatry*, 5(3), e525. <https://doi.org/10.1038/tp.2015.19>
- Wöhr, M., Rouillet, F. I., & Crawley, J. N. (2011). Reduced scent marking and ultrasonic vocalizations in the BTBR T+tf/J mouse model of autism. *Genes, brain, and behavior*, 10(1), 35–43. <https://doi.org/10.1111/j.1601-183X.2010.00582.x>
- Yamada, J., Ohgomori, T., & Jinno, S. (2015). Perineuronal nets affect parvalbumin expression in GABAergic neurons of the mouse hippocampus. *The European journal of neuroscience*, 41(3), 368–378. <https://doi.org/10.1111/ejn.12792>
- Yin, H. H., & Knowlton, B. J. (2004). Contributions of striatal subregions to place and response learning. *Learning & memory (Cold Spring Harbor, N.Y.)*, 11(4), 459–463. <https://doi.org/10.1101/lm.81004>
- Yin, H. H., & Knowlton, B. J. (2006). The role of the basal ganglia in habit formation. *Nature reviews. Neuroscience*, 7(6), 464–476. <https://doi.org/10.1038/nrn1919>
- Yin, H. H., Knowlton, B. J., & Balleine, B. W. (2004). Lesions of dorsolateral striatum preserve outcome expectancy but disrupt habit formation in instrumental learning. *The European journal of neuroscience*, 19(1), 181–189. <https://doi.org/10.1111/j.1460-9568.2004.03095.x>
- Yin, H. H., Knowlton, B. J., & Balleine, B. W. (2005). Blockade of NMDA receptors in the dorsomedial striatum prevents action-outcome learning in instrumental conditioning. *The European journal of neuroscience*, 22(2), 505–512. <https://doi.org/10.1111/j.1460-9568.2005.04219.x>

- Yin, H. H., Ostlund, S. B., Knowlton, B. J., & Balleine, B. W. (2005). The role of the dorsomedial striatum in instrumental conditioning. *The European journal of neuroscience*, *22*(2), 513–523. <https://doi.org/10.1111/j.1460-9568.2005.04218.x>
- Yip, J., Soghomonian, J. J., & Blatt, G. J. (2007). Decreased GAD67 mRNA levels in cerebellar Purkinje cells in autism: pathophysiological implications. *Acta neuropathologica*, *113*(5), 559–568. <https://doi.org/10.1007/s00401-006-0176-3>
- Yizhar, O., Fenno, L. E., Prigge, M., Schneider, F., Davidson, T. J., O'Shea, D. J., Sohal, V. S., Goshen, I., Finkelstein, J., Paz, J. T., Stehfest, K., Fudim, R., Ramakrishnan, C., Huguenard, J. R., Hegemann, P., & Deisseroth, K. (2011). Neocortical excitation/inhibition balance in information processing and social dysfunction. *Nature*, *477*(7363), 171–178. <https://doi.org/10.1038/nature10360>
- Zikopoulos, B., & Barbas, H. (2013). Altered neural connectivity in excitatory and inhibitory cortical circuits in autism. *Frontiers in human neuroscience*, *7*, 609. <https://doi.org/10.3389/fnhum.2013.00609>
- Zwosta, K., Ruge, H., & Wolfensteller, U. (2015). Neural mechanisms of goal-directed behavior: outcome-based response selection is associated with increased functional coupling of the angular gyrus. *Frontiers in human neuroscience*, *9*, 180. <https://doi.org/10.3389/fnhum.2015.00180>

7.0 APPENDICES

Appendix A | *Link and QR code to the recording of mouse brain dissection.*

<https://www.youtube.com/watch?v=SXxqPU9zvgI&t=12s>



Appendix B | *Zeiss Cell Observer Filter Models' Excitation and Detection Wavelengths*

Filter Set	Excitation	Detection
49 DAPI	365	445/50
38 HE eGFP	470/40	525/50
43 HE Cy 3	550/25	605/70

Appendix C | *Average Absorbance of each lysate, concentration ($\mu\text{g}/\mu\text{L}$) determined using the BCA standard curve, and volume of lysate required to obtain 10 μg of proteins (μL).*

Mouse ID	Average Absorbance*	Concentration ($\mu\text{g}/\mu\text{L}$)	Volume for 10 μg of Proteins (μL)
2	1.21625	1.4081	7.1
3	1.12195	1.3006	7.7
6	0.8713	1.0147	9.9
7	1.11475	1.2924	7.7
9	0.97515	1.1332	8.8
11	1.23485	1.4293	7.0
13	0.97945	1.1381	8.8
15	1.2795	1.4803	6.8
19	0.8962	1.0431	9.6
20	0.88475	1.0301	9.7

**Average of two absorbance values and corrected by subtracting blank absorbance*

Appendix D | *Representative Western Blot of Parvalbumin and β -Actin bands, at ~12kDa and ~42kDa respectively, as indicated by molecular weight (kDa) ladder. Achieved by merging imaged bands with a colorimetric image of a prestained protein ladder (10-180kDa; ab116027).*

